

<https://doi.org/10.3799/dqkx.2021.018>



特提斯喜马拉雅东段扎西康矿集区姐纳各普金矿床成因:黄铁矿He-Ar及原位S同位素约束

李洪梁¹, 李光明^{2,3*}, 张志², 张林奎², 董随亮², 卿成实², 李应栩²

1. 中国地质科学院探矿工艺研究所, 四川成都 611734

2. 中国地质调查局成都地质调查中心, 四川成都 610081

3. 成都理工大学地球科学学院, 四川成都 610059

摘要: 姐纳各普金矿床是特提斯喜马拉雅东段扎西康矿集区内新近发现的中新世热液金矿床, 但其成因认识较为模糊。矿体呈层状或似层状, 严格受伸展断裂构造控制, 具蚀变岩型和石英脉型2种矿石, 主要发育硅化、黄铁矿化、绢云母化和方解石化。为厘定矿床成因, 对矿床Ⅱ号和Ⅲ号矿体中的蚀变岩型矿石进行了系统采样, 分析其黄铁矿He-Ar和原位S同位素组成特征。结果表明: 黄铁矿内的⁴He含量介于 0.038×10^{-7} ~ $0.446 \times 10^{-7} \text{ cm}^3 \text{ STP/g}$, 平均含量 $0.200 \times 10^{-7} \text{ cm}^3 \text{ STP/g}$; ³He/⁴He比值介于0.08~0.09 Ra, 平均比值为0.08 Ra; ⁴⁰Ar含量变化于 0.049×10^{-7} ~ $0.132 \times 10^{-7} \text{ cm}^3 \text{ STP/g}$, 平均含量 $0.084 \times 10^{-7} \text{ cm}^3 \text{ STP/g}$; ⁴⁰Ar/³⁶Ar比值介于308.0~386.3, 平均比值347.1, 指示成矿流体主要来自壳源变质流体; 黄铁矿δ³⁴S值分布集中, 总体变化于1‰~3‰, 平均值2.98‰, 显示成矿物质来自地壳深部壳幔物质均一化的深源。结合前人研究成果, 文章认为姐纳各普金矿床属于造山型金矿床, 其成因的厘定对丰富和完善大陆碰撞造山成矿作用理论和指导区域矿床勘查具有重要意义。

关键词: 造山型金矿床; He-Ar同位素; 原位S同位素; 姐纳各普; 扎西康矿集区; 特提斯喜马拉雅; 矿床。

中图分类号: P618.51

文章编号: 1000-2383(2021)12-4291-25

收稿日期: 2020-12-16

Genesis of Jienagepu Gold Deposit in Zhaxikang Ore Concentration Area, Eastern Tethys Himalayas: Constraints from He-Ar and In-Situ S Isotope of Pyrite

Li Hongliang¹, Li Guangming^{2,3*}, Zhang Zhi², Zhang Linkui², Dong Suiliang², Qing Chengshi², Li Yingxu²

1. Institute of Prospecting Technology, Chinese Academy of Geological Sciences, Chengdu 611734, China

2. Chengdu Center of China Geological Survey, Chengdu 610081, China

3. College of Earth Science, Chengdu University of Technology, Chengdu 610059, China

Abstract: Jienagepu gold deposit is a newly discovered Miocene hydrothermal gold deposit in the Zhaxikang ore concentration area, eastern Tethyan Himalayas, but its genesis is rather vague. The ore body is stratified or approximately stratified, strictly

基金项目: 中国地质调查局项目(Nos.DD20190644, DD20190147); 国家自然科学基金项目(Nos.91955208, 41702080, 41602214, 41807300); 国家科学技术部科技支撑计划重点项目(Nos.2016YFC060308, 2018YFC0604103); 第二次青藏高原综合科学考察研究(No.2019QZ-KK0902)。

作者简介: 李洪梁(1990—), 男, 博士, 工程师, 主要从事青藏高原地质矿产勘查评价研究。ORCID:0000-0002-2514-9368. E-mail:siliang2222@126.com

* 通讯作者: 李光明, ORCID:0000-0003-3383-3693. E-mail:li-guangming@163.com

引用格式: 李洪梁, 李光明, 张志, 等, 2021. 特提斯喜马拉雅东段扎西康矿集区姐纳各普金矿床成因: 黄铁矿He-Ar及原位S同位素约束. 地球科学, 46(12):4291—4315.

controlled by extensional fault structure. In this study, two types of ores were recognized, namely altered rock type and quartz vein type, with extensive hydrothermal alternation, including silicification, pyritization, sericization and calcite. Samples were systematically taken from the altered rock type ore in orebody No. II and No. III, and the composition characteristics of He-Ar and in-situ S isotope of pyrite were analyzed to determine the genesis of the deposit. The results show that the content of ${}^4\text{He}$ and ${}^3\text{He}/{}^4\text{He}$ ratio in pyrite ranged widely from $0.038 \times 10^{-7} \text{ cm}^3 \text{ STP/g}$ to $0.446 \times 10^{-7} \text{ cm}^3 \text{ STP/g}$, 0.08 Ra to 0.09 Ra, with an average of $0.200 \times 10^{-7} \text{ cm}^3 \text{ STP/g}$ and 0.08 Ra. The content of ${}^{40}\text{Ar}$ and ${}^{40}\text{Ar}/{}^{36}\text{Ar}$ ratio vary from $0.049 \times 10^{-7} \text{ cm}^3 \text{ STP/g}$ to $0.132 \times 10^{-7} \text{ cm}^3 \text{ STP/g}$, 308.0 to 386.3, with an average of $0.084 \times 10^{-7} \text{ cm}^3 \text{ STP/g}$ and 347.1, indicating that the ore-forming fluid mainly originated from the crustal metamorphic fluid. The $\delta^{34}\text{S}$ value of pyrite is concentrated, and the overall variation is between 1‰ and 3‰, with an average of 2.98‰, showing that the ore-forming material is from crustal-mantle homogenized deep source. Combined with previous research results, in this paper it holds that Jienagepu gold deposit is an orogenic type gold deposit, and the determination of genesis is of great significance to enrich and perfect the mineralization theory of continental collisional orogeny and to guide the exploration of regional ore deposits.

Key words: orogenic gold deposit; He-Ar isotope; in-situ S isotope; Jienagepu; Zhaxikang ore concentration area; Tethys Himalayas; deposit.

0 引言

由印度—欧亚大陆碰撞造山引发的大规模成矿作用在特提斯喜马拉雅构造带(TH)东段形成了众多铅锌金锑矿床,目前已发现各类型铅锌、金(锑)矿床(点)近60处(戚学祥等,2008),如扎西康铅锌多金属矿床、柯月铅锌矿床、吉松铅锌矿床,马扎拉金锑矿床、明赛金矿床、浪卡子金矿床、拉木由塔金矿床,古堆金锑矿床、哲古错金锑矿床,沙拉岗锑矿床、勇日锑矿床等(Yang *et al.*, 2009; 孙晓明等, 2014; 吴建阳等, 2015; Duan *et al.*, 2016; 李洪梁等, 2016, 2017; Sun *et al.*, 2016a; 李光明等, 2017; Xie *et al.*, 2017; 梁维和郑远川, 2019; 谢玉玲等, 2019; Xiang *et al.*, 2020; Zhang *et al.*, 2020),构成了独具特色的藏南铅锌金锑多金属成矿带(聂凤军等, 2005; 杨竹森等, 2006). 该成矿带内以扎西康矿集区最为典型、规模最大,研究程度也最高,代表性矿床即扎西康铅锌多金属矿床和马扎拉金锑矿床. 随着基础地质调查工作的不断推进,中国地质调查局成都地质调查中心扎西康产学研团队以原有的1:5万土壤地球化学资料为基础,在扎西康铅锌多金属矿床西北侧约3 km的姐纳各普地区又新发现了姐纳各普金矿床. 经野外地质填图和探矿工程的揭露与评价发现,姐纳各普金矿床资源量超5 t,达到了中型规模.

作为完善扎西康矿集区成矿系列的重要切入点,姐纳各普金矿床自发现以来就备受关注,先后就其矿床地质特征、流体包裹体、H-O同位素组成和成矿年代学等方面(李洪梁, 2016; 董随亮等,

2017; 李洪梁等, 2017)进行了大量研究,但对成矿物质来源的研究却鲜有涉及,加上石英H-O同位素示踪成矿流体来源存在局限性和主观性(Simon, 2001; Faure, 2003; Grant *et al.*, 2003; Naden *et al.*, 2003; 郭春影等, 2011),导致对于矿床成因的认识较为模糊,成为成矿机制研究亟待解决的关键问题,制约着今后的勘查工作. 因此,深入研究姐纳各普金矿床成因具有重要的理论和现实意义.

稀有气体,尤其是He、Ar,化学性质极不活泼,在经历漫长的地质作用改造后仍能基本保持其源区的初始信息,且具有不同源区He-Ar同位素组成差异显著的特点,被广泛应用于热液金(锑)、铜、铅锌等矿床成矿流体的来源研究(Stuart and Turner, 1992; Stuart *et al.*, 1994a; 胡瑞忠, 1997; Kendrick *et al.*, 2001, 2011); S元素作为热液矿床成矿流体中极为重要的矿化剂,其同位素组成特征是示踪成矿流体中S源的最常用而重要的技术手段之一,具有指示矿床成矿物理化学条件和矿床成因的意义,因而被广泛应用于流体示踪和矿床成因研究(Hoefs, 1997; Adam *et al.*, 2020; Liang *et al.*, 2020; Petrella *et al.*, 2020). 以往S同位素分析方法采用的样品多为硫化物矿石单矿物的粉末,而对于具有多期次叠加成矿的热液矿床而言,往往单矿物提纯难度大或者单个矿物颗粒包含了多期次的成矿流体信息,导致同位素测试结果为一个混合值或变化范围大,难以准确揭示其中隐含的地质信息. 近年来,激光剥蚀和质谱分析技术的出现完美地解决了这一难题,并且已经广泛应用于热液矿床中,取得了良好的效果(赵静等, 2018; 李洪梁等, 2020; 朱照先等, 2020).

因此,笔者在已有研究的基础上,对姐纳各普金矿床主成矿期的载金黄铁矿进行了流体包裹体He-Ar和原位S同位素分析,示踪成矿流体和物质来源,探讨矿床成因,以期深化扎西康矿集区铅锌金锑成矿作用认识,丰富和完善大陆成矿理论。

1 成矿地质背景

喜马拉雅构造带是自新生代以来的印度—欧亚大陆碰撞造山作用的产物(莫宣学和潘桂棠,2006),是全球最年轻、隆升速率最快的巨型大陆碰撞造山带,且目前造山作用过程仍在持续进行中,这也使其成为了研究与大陆碰撞造山作用有关的构造、岩浆、变形变质及成矿作用的天然实验室(侯增谦和王二七,2008)。该构造带夹持于雅鲁藏布江蛇绿混杂岩带(IYS)和主中央边界逆冲断层(MBT)之间,由北向南分别以藏南差离系(STDS)和主中央逆冲断层(MCT)为界,可细分为特提斯喜马拉雅(TH)、高喜马拉雅(HH)和低喜马拉雅(LH)3个次级构造单元(图1a)。其中,特提斯喜马拉雅构造带(TH)形成于印度板块的持续向北俯冲,并以洛生长断层为界,主要由北侧的中生界被动大陆边缘沉积岩系和南侧的早古生代火山岩、沉积岩以及石炭系—侏罗系台地相碳酸盐岩—碎

屑岩组成(图1b)(杨竹森等,2006;潘桂棠等,2009)。受碰撞造山作用影响,带内地层内多发育轴向为东西向的复式褶皱及走向近东西的断裂,并被南北向裂谷系穿切。除此之外,在后碰撞伸展阶段(<25 Ma;侯增谦等,2006a),由基底隆升使地壳减压熔融,在特提斯喜马拉雅构造带(TH)北侧及藏南拆离系(STDS)内形成了两条近乎平行的、东西向展布的淡色花岗岩带,分别为特提斯喜马拉雅淡色花岗岩带和高喜马拉雅淡色花岗岩带,两者在矿物组合、岩石类型和地球化学特征上极为相似,具有同源的特点,属高分异的S型花岗岩(张进江和丁林,2003;张进江,2007;张进江等,2007;吴福元等,2015;Fu et al., 2017;黄春梅等,2018;Wu et al., 2020;Xie et al., 2020)。

扎西康矿集区位于特提斯喜马拉雅构造带东段(图1b),受早期近南北向印度—欧亚大陆碰撞造山作用和晚期东西向伸展作用的叠加影响,区内主体构造线呈近东西向或北西西—南东东向展布,并被晚期南北向裂谷系及相关正断层穿切(图2)。矿集区内内地层出露简单,主要为一套未变质—弱变质的侏罗系海相细碎屑岩夹碳酸盐岩、火山岩(主要为凝灰岩)和硅质岩建造。矿集区岩浆活动强烈,除广泛分布的白垩纪双峰式火山岩外,主要为新近厘

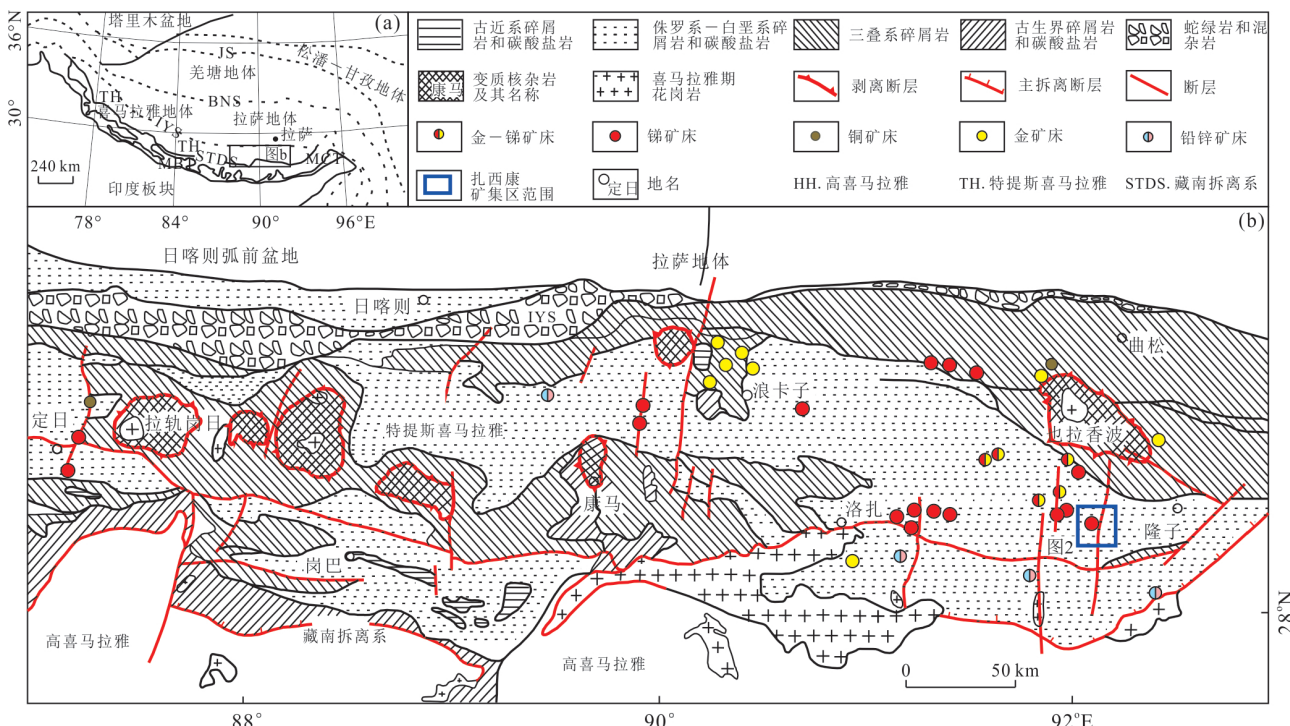


图1 研究区大地构造位置(a)及区域矿床分布图(b)(据杨竹森等,2006修改)

Fig.1 Geotectonic (a) and regional deposit distribution (b) maps of the study area(modified from Yang et al., 2006)

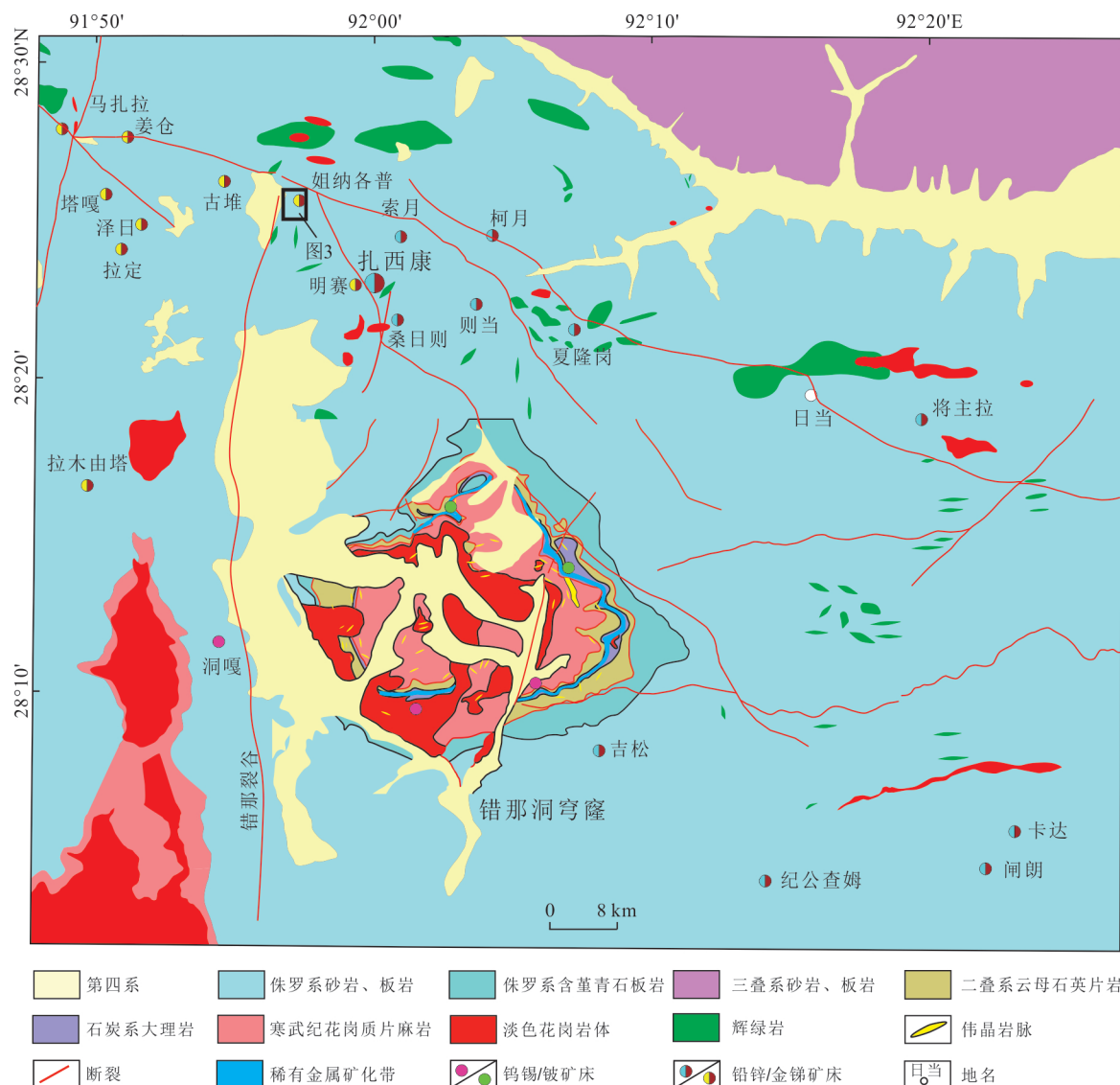


图2 扎西康矿集区地质图(据李光明等,2017修改)

Fig.2 Geological map of Zhaxikang ore concentration area (modified from Li et al., 2017)

定的错那洞淡色花岗岩穹窿。穹窿内岩性组合较为复杂,可见含石榴子石花岗岩、电气石榴花岗岩和二云母花岗岩等,并具有多期次侵入的特点,侵位年龄介于21~14 Ma,岩石地球化学分析显示其源岩为变泥质岩,其形成与藏南拆离系(STDS)启动诱发的构造减压密切相关(李光明等,2017;付建刚等,2018;黄春梅等,2018;张林奎等,2018,2019)。

2 矿床地质特征

2.1 矿区地质特征

姐纳各普金矿床位于扎西康矿集区西北侧(图2),矿区地层岩性出露简单,除第四系(Q)残、坡积物外,主要为下—中侏罗统陆热组一段(J_{1-2}^L)钙质

板岩、陆热组二段(J_{1-2}^L)薄层泥灰岩夹凝灰岩条带和中侏罗统遮拉组(J_2^Z)粉砂质板岩。矿区构造线总体特征与矿集区近于一致,早期构造线总体呈北西—南东向展布,被后期东西向伸展作用形成的南北向断裂构造切割(图3)。早期构造总体表现为一系列北西—南东向的复式同斜倒转褶皱以及两翼地层中的层间破碎带。破碎带产状总体与上、下盘地层产状一致,主要由破碎的凝灰岩组成,且具有早期压扭、晚期伸展拉张的多期次活动特点,为印度—欧亚大陆碰撞作用过程中伴随褶皱形成的压扭性封闭裂隙在后期伸展过程中发生伸展滑脱而形成,其拉张扩容空间为金矿床主要的容矿构造。矿区内地层分布广泛,但规模较小,主要为顺层分布的燕山期辉绿岩脉,受碰撞造山影响,多呈“M”

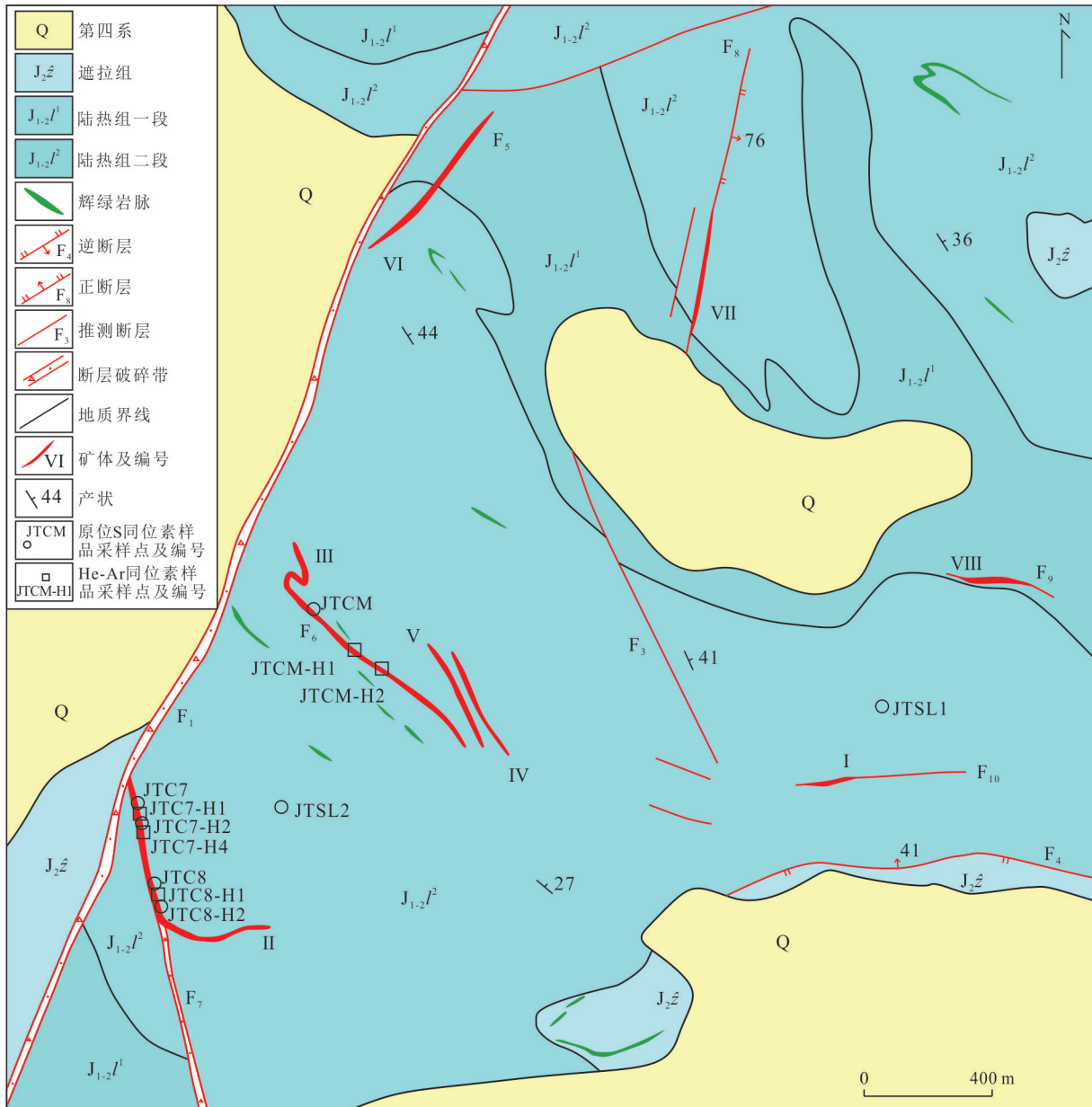


图3 姐纳各普金矿区地质图

Fig.3 Geological map of Jienagepu gold mining area

或“S”型被卷入同斜倒转褶皱中。

2.2 矿体与矿石特征

通过野外地质填图、实测剖面以及探槽、剥土和钻孔等探矿工程的研究发现,矿(化)体主要产于早期挤压背景形成的同斜倒转褶皱两翼的层间破碎带中,极少数矿(化)体分布在近东西向的断裂中,其中这些层间破碎带在晚期又受到了伸展滑脱的影响。目前,勘查工作已发现8条金矿(化)体。矿体主要呈长透镜状或似层状,各矿(化)体详细的地质产状与分布特征详见表1,其中规模最大的为分布在矿区西南部和西部的Ⅱ号和Ⅲ号矿体。

其中,Ⅱ号矿体整体呈北北西向展布于矿区西南部,受 F_7 断裂及层间破碎带控制,赋矿岩石为破碎带中的蚀变凝灰岩,顶、底板围岩岩性均为下—中侏罗统陆热组二段($J_{1-2}l^2$)灰黑色钙质板岩、薄层泥灰岩,其间有品位较低断层泥。矿体呈似层状,严格受北西西—南东东向正断层控制(图4),矿体南段受同斜褶皱的影响而出现转弯(图3),总体产状 $65^\circ \angle 20^\circ$,走向延伸近1 000 m,斜深大于200 m。矿体厚度变化于5.66~22.05 m,平均厚度12.07 m;矿体品位变化于1.05~10.61 g/t,平均品位2.03 g/t。按照矿石工业类型划分,可见蚀变岩型和石英脉型

表 1 姐纳各普金矿床主要矿(化)体地质特征

Table 1 Geological characteristics of main ore (mineralized) bodies of Jienagepu gold deposit

矿 (化) 体编 号	位置	矿石工业类型	矿石组构	矿(化)体			矿(化)体规模		品位(g/t)
				矿(化) 体形态	产状	走向延 伸(m)	厚度(m)		
(°)	(°)								
I	矿区 东南	蚀变岩型	碎裂、土状结构;角砾状构造	透镜状	152	72	~100	1.12~2.16	0.11~9.67
II	矿区 西南	石英脉型、蚀变岩型	交代、碎裂结构;网脉状、角砾状、及晶洞构造	似层状 透镜状	65	20	~1 000	5.66~22.05	1.05~10.61
III	矿区 西部	石英脉型、蚀变岩型	交代、碎裂结构;网脉状、角砾状、及晶洞构造	似层状 透镜状	57~ 68	27~ 43	>1 000	1.21~3.21	0.98~2.94
IV	矿区 中部	蚀变岩型	碎裂结构;角砾状构造	似层状	64	41	260	1.01~2.26	0.28~1.94
V	矿区 中部	蚀变岩型	碎裂结构;角砾状构造	似层状	69	38	220	1.21~3.21	0.94~1.18
VI	矿区 北部	蚀变岩型	碎裂结构;角砾状构造	似层状 透镜状	118	40	>600	1.14~3.62	0.22~2.65
VII	矿区 东北	蚀变岩型	碎裂结构;角砾状构造	似层状	90	70	~60	1.92	0.22~2.65
VIII	矿区 东部	石英脉型、蚀变岩型	交代、碎裂结构;网脉状、角砾状及晶洞构造	似层状	355	70	~130	1.98	1.35~9.76

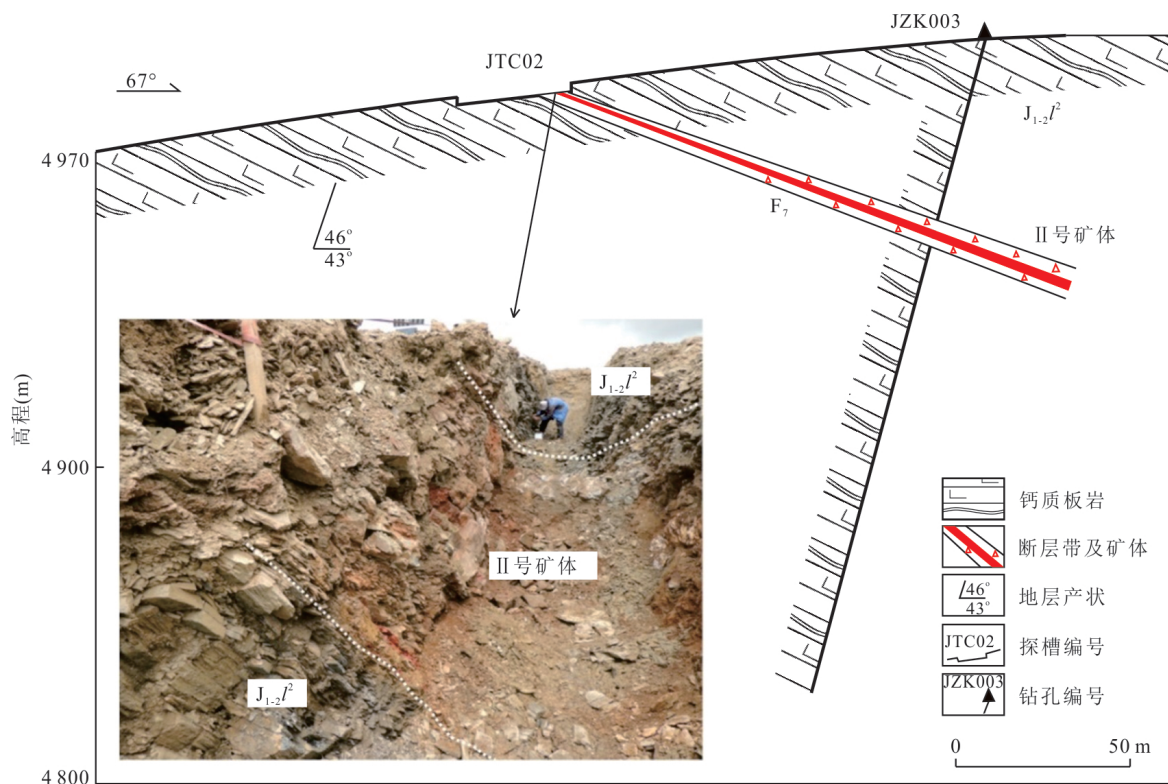


图 4 姐纳各普金矿床 3 号勘探线剖面

Fig.4 Section of No.3 exploration line of Jienagepu gold deposit

2 种矿石, 矿石中可见大量含金石英脉或网脉, 具块状、网脉状(图 5a)、角砾状(图 5b)和土状构造, 粒

状、溶蚀、碎裂结构, 主要矿石矿物包括自然金(图 5c)、方铅矿、闪锌矿(图 5d)、辉锑矿、辰砂(图 5e)、

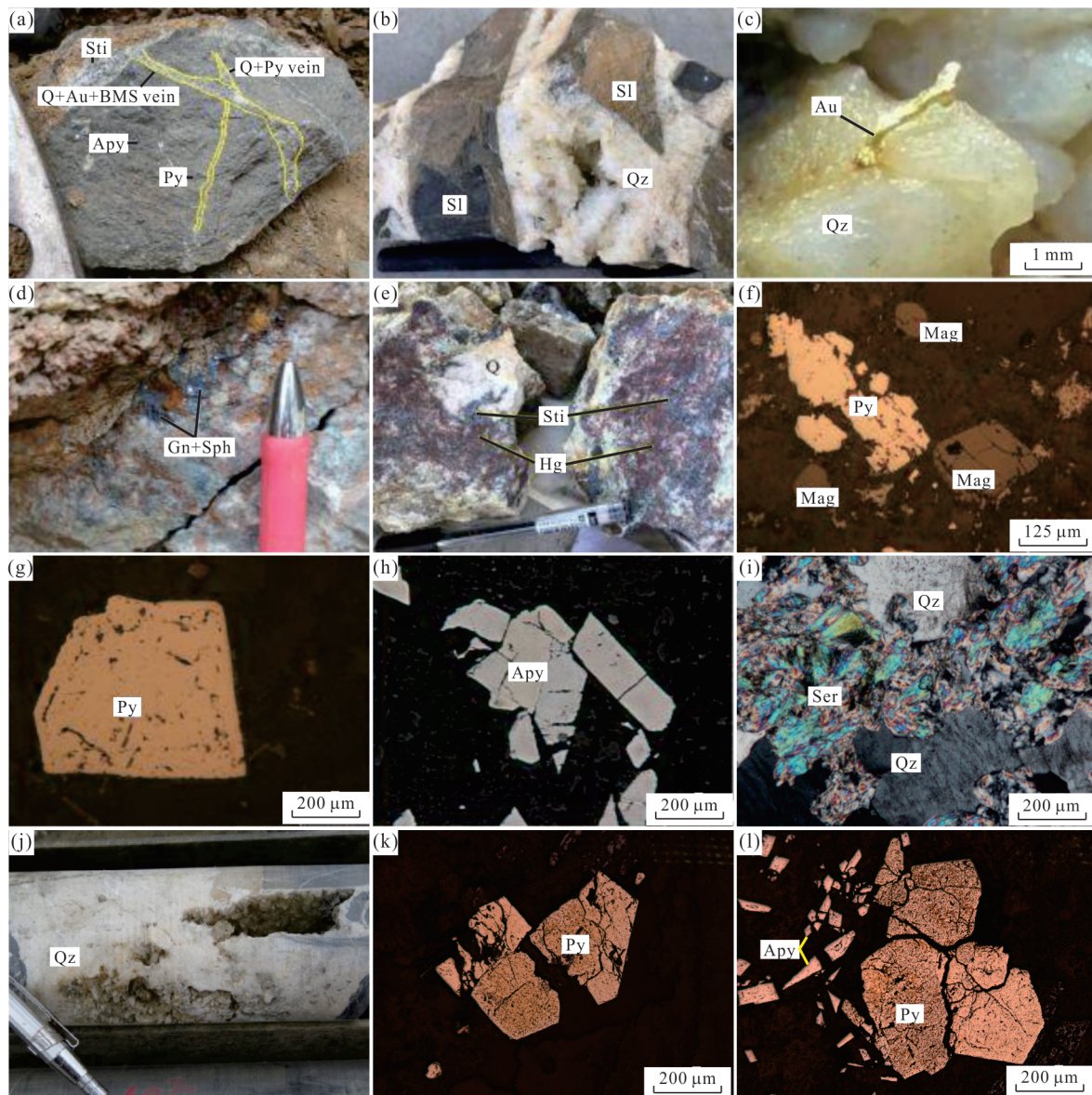


图5 姐纳各普金矿床主要矿石矿物特征

Fig.5 Main ore mineral characteristics of Jienagepu gold deposit

a. 蚀变岩型矿石及穿切其中石英—硫化物脉;b. 石英脉型矿石中发育的角砾状、晶洞及晶簇构造;c. 石英脉型矿石中的自然金;d. 方铅矿与闪锌矿集合体;e. 石英脉型矿石中的辉锑矿及薄膜状辰砂;f. 半自形黄铁矿及磁铁矿颗粒;g. 具微弱环带结构的自形粒状黄铁矿颗粒;h. 自形板状毒砂颗粒;i. 石英脉型矿石中发育的硅化与绢云母化;j. 石英脉型矿石中的晶洞、晶簇构造;k. 自形粒状黄铁矿颗粒;l. 半自形—自形粒状黄铁矿颗粒及自形菱面体、板状毒砂颗粒;Qz. 石英;Apy. 毒砂;Py. 黄铁矿;BMS. 贱金属硫化物;Sti. 辉锑矿;Gn. 方铅矿;Sph. 闪锌矿;Hg. 辰砂;Mag. 磁铁矿;Ser. 绢云母

黄铁矿、毒砂(图5f~5h)及少量的磁铁矿(图5f),脉石矿物主要为石英、绢云母(图5i)和方解石。

Ⅲ号矿体于矿区西部地区,呈北西—南东向分布,主要赋存于北西—南东向的F₆层间破碎带内。矿体呈层状或似层状,沿顺层的层间破碎带曲折延伸,矿体产状56°~68°/27°~43°,变化较大。矿体厚度介于1.21~3.21 m,平均厚度1.75 m;矿体品位变化于0.98~2.94 g/t,平均品位1.58 g/t。矿石主要以

石英脉型为主,多见角砾状、块状、晶洞和晶簇构造(图5j),自形一半自形粒状结晶结构,其中矿石矿物主要为自然金以及黄铁矿、毒砂等(图5k和5l),脉石矿物主要为绢云母、石英、方解石等。

2.3 围岩蚀变与成矿期次

姐纳各普金矿区围岩蚀变发育,总体表现为一套以硅化、绢云母化、黄铁矿化、毒砂化、碳酸盐化为主的中—低温热液蚀变。根据脉体交切关系、矿

石结构以及矿物共生组合特征,可将姐纳各普金矿床成矿过程划分为早期原生热液成矿期和晚期表生风(氧)化成矿期。按照矿物生成顺序,原生热液成矿期又依次分为石英—黄铁矿阶段(早)、石英—金—贱金属硫化物阶段(中)和石英—碳酸盐矿物阶段(晚)。其中,早阶段为成矿热液沿着先成的构造裂隙交代围岩,仅有少量呈微—细粒的自形立方体状黄铁矿颗粒形成,矿化较弱;中阶段为主要的金矿化阶段,为主成矿阶段,形成了大量石英—金—贱金属硫化物脉,并进一步交代、胶结早期破碎的凝灰岩,形成大量毒砂、黄铁矿等,而且这些金属硫化物结晶颗粒较大;晚阶段基本无矿化,形成穿切早期脉体的石英一方解石脉。

3 样品采集与分析方法

本次研究所涉及的样品均采集于控制姐纳各普金矿床Ⅱ号和Ⅲ号矿体的探槽和钻孔中的蚀变岩型金矿石。对野外样品进行系统编号后,选取石英—金—贱金属硫化物阶段(主成矿阶段)的样品在中国地质调查局成都地质调查中心进行制片和岩矿鉴定,并对余样进行黄铁矿单矿物挑选,挑选纯度大于99%。

黄铁矿流体包裹体He-Ar同位素分析测试工作在核工业北京地质研究院完成。测试仪器采用美国 Thermo Fisher 公司生产的 Helix SFT 稀有气体同位素质谱仪。该仪器由超高真空压碎装置、高温熔样炉、气体纯化系统和稀有气体同位素质谱测试系统组成,可实现³He 和⁴He 同时接收,是 He 同位素分析的专用仪器,主要用于矿物包裹体等样品中稀有气体同位素比值(³He/⁴He, ⁴⁰Ar/³⁶Ar 等)分析,并有能力分析所有稀有气体(He、Ne、Ar、K_e、Xe)的同位素组成。该仪器在超高真空状态下运行,样品处理系统的真空为 $5 \times 10^{-9} \sim 10 \times 10^{-9}$ mbar, 质谱系统真空达 $7 \times 10^{-9} \sim 9 \times 10^{-10}$ mbar。仪器内部体积小, 约 1 400 cc, 灵敏度高。对³He 测定分辨率大于 700,³He 和 HD 峰可以完全分开, 丰度灵敏度在 1×10^{-7} mbar, 真空下 30 min 内小于 1×10^{-9} mbar。测试前,首先粉碎并筛选出 40~60 目的样品,依次用乙醇、去离子水和丙酮超声清洗,除去样品表面吸附的杂质,设定温度为 120 ℃烘干。烘干后,称取 2~3 g 的样品,放置压碎装置内,将装置全金属密封后在 250 ℃条件下烘烤 48 h,同时用无油分子泵组进行抽真空,除去压碎装置腔体及样品表面吸附气体。

去气结束后,调用 He 同位素测量离子源参数,并稳定 30 min,依次测量整套系统本底值,标准氦气同位素组成值,然后压碎样品,对样品进行纯化、测量。

黄铁矿原位 S 同位素测试分析在西北大学大陆动力学国家重点实验室进行。激光剥蚀系统是 193 nm 准分子激光剥蚀系统(Resolution M-50, ASI),包含一台 193 nm ArF 准分子激光器,一个双室样品室和电脑控制的高精度 X-Y 样品台移动、定位系统。双室样品池能有效避免样品间交叉污染,减少样品吹扫时间,同时装载样品能力大大提高,减少了频繁换样过程中人为因素的影响。测试 S 同位素时使用的激光能量密度(Fluence)为 3.6 J/cm²,频率(Frequency)为 3 Hz,剥蚀斑束(Spot Size)为 25~37 μm,剥蚀方式为单点剥蚀,载气为高纯氦气(280 mL/min),补充气体为 Ar,一般为 0.86 L/min。S 同位素分析采用多接收等离子体质谱(Nu Plasma 1700 MC-ICP-MS),NP-1700 则有 10 个固定的法拉第杯和 6 个可移动的法拉第杯(高、低质量端各有 3 个)以及 3 个离子计数器组成。法拉第杯 H5、Ax 和 L4 分别接收 34 s、33 s 和 32 s。通过调节源狭缝、X-Y 狹缝以及法拉第杯前可调节的 collector slit 可得到大于 20 000 的分辨率(Resolution Power)。测试 S 同位素一般使用的分辨率大于 12 000,此时 Nu 1700 能将 32 s 与干扰(¹⁶O-¹⁶O)分开,测试 δ³⁴S 可达很高的精度(小于 0.1‰)。数据采集模式为 TRA 模式,积分时间为 0.2 s,背景采集时间为 30 s,样品积分时间为 50 s,吹扫时间为 75 s。详细的测试流程见 Bao *et al.* (2017)、Chen *et al.* (2017) 和 Yuan *et al.* (2018) 所述。

4 测试结果

4.1 He-Ar 同位素组成

姐纳各普金矿床 5 件黄铁矿样品测试结果如表 2 所示。从表 2 中可见,黄铁矿流体包裹体内的⁴He 含量介于 $0.038 \times 10^{-7} \sim 0.446 \times 10^{-7}$ cm³ STP/g (Standard Temperature and Pressure, STP, 标准温度与标准压强,简称“标况”,表示温度为 0 ℃、压强为 101.325 kPa 时的状况),平均含量 0.200×10^{-7} cm³ STP/g;³He/⁴He 比值介于 0.08~0.09 Ra 之间(Ra=1.399×10⁻⁶,代表大气中的³He/⁴He 比值),平均比值约为 0.08 Ra;⁴⁰Ar 含量变化于 $0.049 \times 10^{-7} \sim 0.132 \times 10^{-7}$ cm³ STP/g, 平均含量 0.084×10^{-7} cm³ STP/g;⁴⁰Ar/³⁶Ar 比值介于 308.0~386.3, 平均比值 347.1;³⁸Ar/³⁶Ar 比值介于 0.188~5~

表2 姐纳各普金矿床黄铁矿He-Ar同位素组成
Table 2 Isotopic compositions of He-Ar in pyrite from Jienagepu gold deposit

样品号	JTCM-H1	JTCM-H2	JTC7-H1	JTC7-H4	JTCM-H1
所属矿体编号	Ⅲ号	Ⅲ号	Ⅱ号	Ⅱ号	Ⅱ号
矿石类型	蚀变岩型	蚀变岩型	蚀变岩型	蚀变岩型	蚀变岩型
测试矿物	黄铁矿	黄铁矿	黄铁矿	黄铁矿	黄铁矿
⁴ He(cm ³ STP/g) E-7	0.360	0.446	0.042	0.115	0.038
⁴⁰ Ar(cm ³ STP/g) E-7	0.081	0.100	0.049	0.132	0.057
³ He/ ⁴ He(Ra)	0.08	0.08	0.08	0.09	0.09
⁴⁰ Ar/ ³⁶ Ar	386.3	381.6	331.5	328.0	308.0
³⁸ Ar/ ³⁶ Ar	0.189	0.189	0.189	0.189	0.189
⁴⁰ Ar/ ⁴ He	0.22	0.22	1.15	1.15	1.50
幔源He(%)	0.93	0.93	0.93	1.08	1.08
⁴⁰ Ar*(%)	23.51	22.56	10.86	9.91	4.06
⁴⁰ Ar*(cm ³ STP/g) E-7	0.019	0.023	0.005	0.013	0.002
⁴⁰ Ar*/ ⁴ He	0.053	0.051	0.125	0.114	0.061
F ⁴ He	10 458	10 316	1 742	1 732	1 247

注:幔源He(%)=[(³He/⁴He)_{样品}-(³He/⁴He)_{大气}]/[³He/⁴He]_{地幔}-(³He/⁴He)_{大气}]×100; ⁴⁰Ar*(%)=[(⁴⁰Ar/³⁶Ar)_{样品}-295.5]/(⁴⁰Ar/³⁶Ar)_{样品}×100; ⁴⁰Ar*=⁴⁰Ar×[1-(⁴⁰Ar/³⁶Ar)_{大气}/(⁴⁰Ar/³⁶Ar)_{样品}]; F⁴He=(⁴He/³⁶Ar)_{样品}/(⁴He/³⁶Ar)_{大气}.

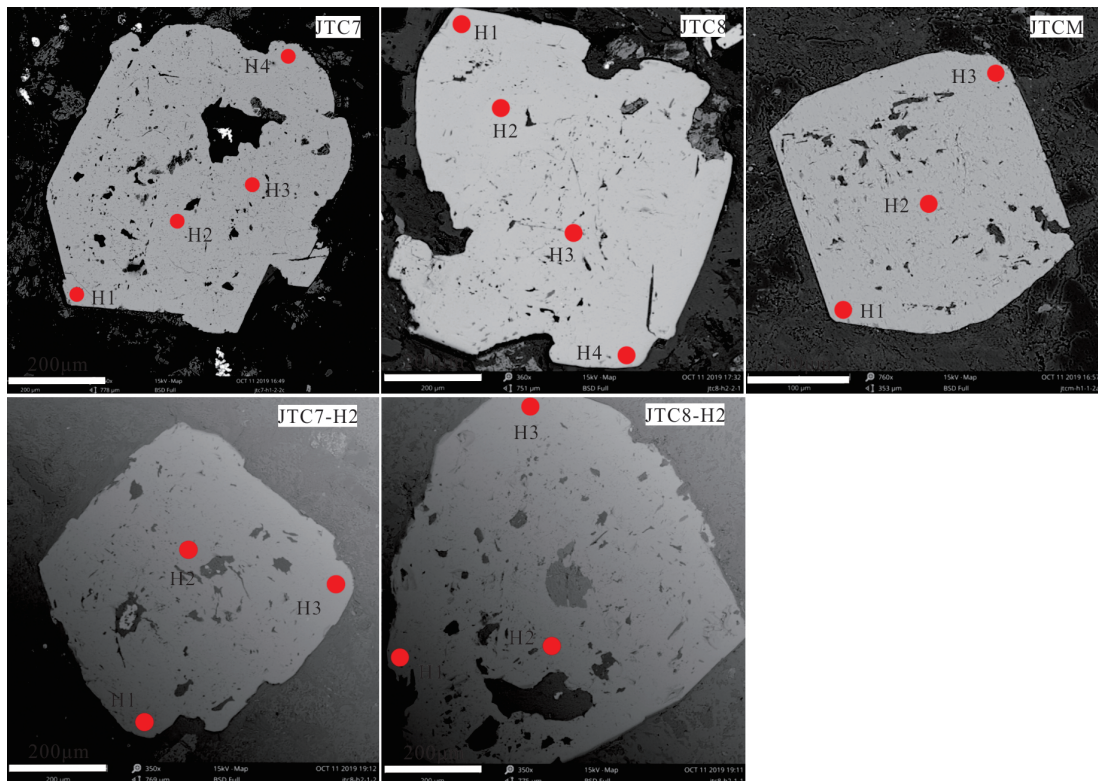


图6 黄铁矿背散射照片及原位S同位素测点分布

Fig.6 BSE photographs of pyrite and distribution of in-situ S measurement points
红色圆圈表示测点位置及编号

0.189 3,平均比值0.188 9.

4.2 原位S同位素组成

为便于对比分析,本次研究工作对7件黄铁矿

样品、累计19个测点进行了原位S同位素测试。其中包括5件蚀变岩型矿石样品、累计17个测点和2件陆热组(J₁₋₂)钙质板岩样品、各1个测点。5件蚀变

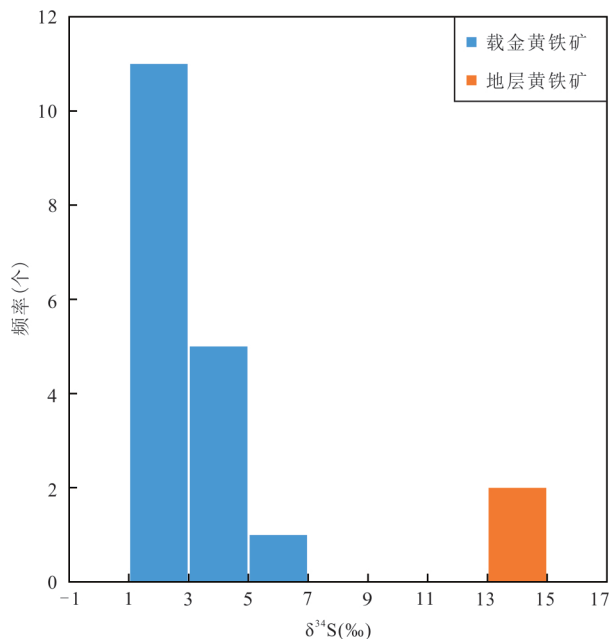


图 7 姐纳各普金矿床原位 S 同位素组成直方图

Fig.7 Histogram of in-situ S isotopic composition of Jienagepu gold deposit

岩型矿石样品中的测点分布如图 6 所示,所有样品测试结果如表 3 所示。

从表 3 可见,姐纳各普金矿床中 17 个测点的 $\delta^{34}\text{S}$ 值分布集中,总体变化于 $1.23\text{\textperthousand} \sim 5.46\text{\textperthousand}$ 之间,平均为 $2.98\text{\textperthousand}$,极差为 $4.23\text{\textperthousand}$ 。在频率直方图(图 7)上可见, $\delta^{34}\text{S}$ 值也表现出集中分布的特点,多介于 $1\text{\textperthousand} \sim 3\text{\textperthousand}$ 。其中,JTCM 样品 3 个测点的 $\delta^{34}\text{S}$ 值明显高于其余样品,介于 $4.77\text{\textperthousand} \sim 5.46\text{\textperthousand}$,平均为 $5.07\text{\textperthousand}$,极差为 $0.69\text{\textperthousand}$;另外,2 件地层黄铁矿样品的 $\delta^{34}\text{S}$ 值相当,明显高于蚀变岩型含金矿石样品,分别为 $14.46\text{\textperthousand}, 14.79\text{\textperthousand}$,平均为 $14.62\text{\textperthousand}$,极差为 $0.33\text{\textperthousand}$ 。

需要说明的是,尽管 5 件样品中黄铁矿在反射光(图 5G)及背散射(BSE)照片(图 6)中均可见具有微弱的环带特征,但各测点分析结果分布集中(图 7),表明尽管成矿热液活动是“脉动”的,但其性质并未发生明显改变,故在此不分期次描述及后续讨论。

5 讨论

5.1 成矿流体来源

He、Ar 等稀有气体在矿物中的存在形式主要有 3 种:(1) 矿石矿物的流体包裹体之中;(2) 矿石矿物流体包裹体或矿物晶格间的 U、Th 和 K 等放射性

表 3 姐纳各普金矿床黄铁矿原位 S 同位素组成

Table 3 Isotopic compositions of S in pyrite from Jienagepu gold deposit

样品 编号	所属矿 体编号	岩性	测试 矿物	测点编号	$\delta^{34}\text{S}$ (‰)
JTC7 II 号		蚀变岩型含金 矿石	黄铁矿	JTC7-H1	4.49
		蚀变岩型含金 矿石	黄铁矿	JTC7-H2	1.80
		蚀变岩型含金 矿石	黄铁矿	JTC7-H3	1.23
		蚀变岩型含金 矿石	黄铁矿	JTC7-H4	2.20
JTC8 II 号		蚀变岩型含金 矿石	黄铁矿	JTC8-H1	4.78
		蚀变岩型含金 矿石	黄铁矿	JTC8-H2	2.20
		蚀变岩型含金 矿石	黄铁矿	JTC8-H3	2.48
		蚀变岩型含金 矿石	黄铁矿	JTC8-H4	3.64
JTCM III 号		蚀变岩型含金 矿石	黄铁矿	JTCM-H1	4.98
		蚀变岩型含金 矿石	黄铁矿	JTCM-H2	5.46
		蚀变岩型含金 矿石	黄铁矿	JTCM-H3	4.77
JTC8-H2 II 号		蚀变岩型含金 矿石	黄铁矿	JTC8-H2-2-1	1.39
		蚀变岩型含金 矿石	黄铁矿	JTC8-H2-2-2	1.91
		蚀变岩型含金 矿石	黄铁矿	JTC8-H2-2-3	2.65
JTC7-H2 II 号		蚀变岩型含金 矿石	黄铁矿	JTC7-H2-2-1	1.98
		蚀变岩型含金 矿石	黄铁矿	JTC7-H2-2-2	2.29
		蚀变岩型含金 矿石	黄铁矿	JTC7-H2-2-3	2.39
JTSL1	围岩	钙质板岩	黄铁矿	JTSL1-1	14.79
JTSL2	围岩	钙质板岩	黄铁矿	JTSL2-1	14.46

元素衰变形成 ${}^4\text{He}$ 、 ${}^{40}\text{Ar}$;(3) 矿石矿物表面或者裂隙吸附的大气中的 He、Ar(Mamyrin and Tolstikhin, 1984; Andrews, 1985; Kurz, 1986)。已有的研究资料证实,热液矿床形成的金属硫化物中的 He、Ar 等稀有气体主要赋存于其内部的流体包裹体之中,但由于金属硫化物形成之后的稀有气体加入或者扩散丢失,宇宙射线或核反应形成的 ${}^3\text{He}$ 的混入,或(和)

金属硫化物中自身携带的放射性元素衰变产生的⁴He、⁴⁰Ar的累积等诸多因素,均会导致其内部的He-Ar同位素组成发生改变(Turner and Stuart, 1992; Stuart *et al.*, 1994a; Hu *et al.*, 1998, 2009; Burnard *et al.*, 1999; Burnard and Polya, 2004).

研究显示,由宇宙射线形成的³He仅分布在地表1.5 m的范围(Kurz, 1986),而本次研究所涉及的黄铁矿样品均来自大于1.5 m的探槽和钻孔内,因此可排除宇宙射线的影响.同时,尽管Li、U和Th的衰变可形成³He,K的衰变可形成⁴⁰Ar(Mamyrin and Tolstikhin, 1984),但这些元素在黄铁矿内的含量极低,并且姐纳各普金矿床成矿为年轻的中新世(17.6±1.8 Ma;董随亮等,2017),因此放射性衰变产生的³He和⁴⁰Ar可完全忽略不计(Pettke and Frei, 1996; Burnard *et al.*, 1999; Kendrick and Burnard, 2013).再者,与赋存于流体包裹体中的Ar相比,矿石矿物中有放射性产生的⁴⁰Ar更是微不足道,其成岩成矿后的扩散和丢失亦可忽略不计(Burnard and Polya, 2004).研究表明,黄铁矿和辉锑矿等金属矿物对稀有气体He具有天然良好的保存能力,即使经历了10~1 000 Ma的样品仍能保持其原有的He-Ar同位素组成,如晚古生代的阿希金金矿床、Panasqueira铜钨锡矿床和新生代的跳玲钨床(Turner and Stuart, 1992; 翟伟等, 2012; Kendrick and Burnard, 2013).因此,表2所罗列的He-Ar同位素组成数据可代表姐纳各普金矿床成矿流体被捕获时的He-Ar同位素组成.

鉴于稀有气体在地幔、地壳岩石和大气圈内具有显著区别的He-Ar同位素组成而被广泛应用于成矿流体来源的示踪(Simmons *et al.*, 1987).为示踪成矿流体的具体来源,本次研究对姐纳各普金矿床进行了黄铁矿流体包裹体He-Ar同位素组成剖析.对于幔源流体,可细分为源于大陆岩石圈地幔和大洋岩石圈地幔的流体2种,前者³He/⁴He比值为6~8 Ra,后者为7~9 Ra,幔源Ar则主要以放射成因的⁴⁰Ar*为主,其⁴⁰Ar/³⁶Ar比值多大于40 000(Porcelli *et al.*, 1992; Patterson *et al.*, 1994; Reid and Graham, 1996),而与弧相关的幔源流体⁴⁰Ar/³⁶Ar比值则介于400~1 000(Kendrick *et al.*, 2002a, 2006);对于壳源流体,由于地壳岩石内含有大量的大离子亲石元素,可形成核成因或放射成因的He,因此其³He/⁴He比值小于0.1 Ra(Andrews, 1985),但⁴⁰Ar/³⁶Ar比值则变化性较大,可分布在n×

$10^2 \sim n \times 10^4$ 之间,这主要与壳源岩石岩性、K含量、复变质作用类型、成岩/成矿年龄和构造环境相关(Ozima and Podosek, 1983; Torgersen, 1989; Kendrick *et al.*, 2001, 2002a, 2002b, 2005, 2006, 2007, 2008, 2011);对于改造型大气饱和水或建造水,在一定温压条件下,大气与其处于平衡状态,因此与大气圈具有相似的He-Ar同位素组成,即³He/⁴He比值约为 1.399×10^{-6} ,⁴⁰Ar/³⁶Ar比值为295.5.值得注意的是,由于空气中的He含量极低,在水溶液中的溶解度更是最低的稀有气体,因此建造水中的He含量更低,其He/Ar比值约 1×10^{-4} (Simmons *et al.*, 1987; Burnard *et al.*, 1999).对于稀有气体Ar,由于其在大气中含量较高,而且在岩石中的封闭温度也要远远高于He,因此浅层次地下水或地表水中基本不含放射成因Ar,与大气具有相同的Ar同位素组成.然而,在地下含水层中由于Th和U等放射性元素的衰变会形成⁴He而不断进入地下水,因此导致其³He/⁴He比值低于大气中的³He/⁴He比值,所以改造型大气饱和水或建造水具有³He/⁴He低比值以及与大气接近的⁴⁰Ar/³⁶Ar比值(Ballentine and Burnard, 2002).

在图8中,姐纳各普金矿床及扎西康矿集区内的马扎拉金锑矿床(张刚阳, 2012; 翟伟等, 2018)、明赛金矿床(Zhang *et al.*, 2020)与分布在雅鲁藏布江缝合带(IYS)内及边缘的典型造山型金矿床(韦慧晓等, 2010; 张刚阳, 2012; Zhou *et al.*, 2014; Sun *et al.*, 2016b)一样,全部投点于幔源He与壳源He之间,靠近壳源He的区域,但较分布在雅鲁藏布江缝合带(IYS)内及边缘的典型造山型金矿床更靠近壳源He区域,显示成矿流体以壳源成矿流体为主,暂不排除有幔源成矿流体参与的可能性.

从³He/⁴He比值来看,所有样品的³He/⁴He比值均小于地壳岩石的³He/⁴He比值上限0.1 Ra(Simmons *et al.*, 1987),显示成矿流体为壳源流体,基本无幔源流体参与成矿.同时,姐纳各普金矿床流体包裹体研究显示,成矿流体属于含有有机质的中温、低盐度、低密度、富集CO₂的H₂O-NaCl-CO₂-CH₄-N₂体系(李洪梁等, 2017),这明显区别于基本不含有有机气体的高温、高盐度岩浆热液(陈衍景等, 2007; 卢焕章等, 2008, 2018; 周云等, 2011),表明岩浆流体参与成矿的可能性较小或极为微弱.另外,Goldfarb and Groves(2015)对变质流体的H-O同位素组成研究发现,尽管其δD值因变化性大而难以解释,

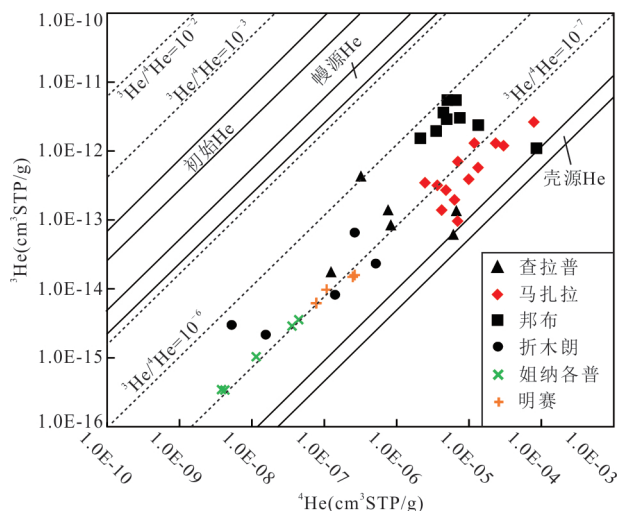
图 8 姐纳各普金矿床黄铁矿³He—⁴He图解

Fig.8 ³He—⁴He diagram of pyrite in Jinaigop gold deposit. Bottom map data from Mamyrin and Tolstikhin (1984); Chalapu data from Zhang et al. (2012); Mazarla data from Zhang et al. (2012) and Zhou et al. (2018); Zhemulang data from Zhou et al. (2014); Bangbu data from Wei et al. (2010) and Sun et al. (2016b); Mingse data from Zhang et al. (2020).

但其 $\delta^{18}\text{O}$ 值一般介于7‰~13‰。李洪梁等(2016)对Ⅱ号矿体含金石英脉矿石中石英进行的H-O同位素测试结果显示,δD值介于-142.9‰~-128.0‰,平均为-139.0‰;δ¹⁸O值介于7.7‰~12.8‰,平均10.5‰。其中,矿床δD值落入与西藏大气降水范围(-150‰~-18‰;郑淑蕙等,1982),暗示大气降水参与了成矿,而δ¹⁸O值与变质流体的δ¹⁸O值近于一致,表明成矿流体为大气降水与变质流体混源。

前已述及,由于He在水体中的溶解度极低,因此改造成型大气饱和水或建造水中的³He/³⁶Ar比值一般低于 1×10^{-7} ,对成矿流体中同位素组成的影响可忽略不计,因此成矿流体中He的来源主要为地幔和地壳(Burnard and Polya, 2004)。姐纳各普金矿床所有样品的F⁴He值[F⁴He = (⁴He/³⁶Ar)_{样品}/(⁴He/³⁶Ar)_{大气}] (Ballentine and Burnard, 2002)介于1 247~10 458,平均为5 099,意味着样品中的⁴He含量至少是大气中⁴He含量的1 247倍,因此大气⁴He对成矿流体的贡献亦可忽略不计。

按照幔—壳二元体系估算He含量的经验公式:He_{地幔}(%)=[(³He/⁴He)_{样品}—(³He/⁴He)_{地壳}]/[³He/⁴He]_{地幔}—(³He/⁴He)_{地壳}]×100(Ballentine and Burnard, 2002),其中(³He/⁴He)_{地壳}代表地壳岩石的平均产物,取值0.02 Ra;(³He/⁴He)_{地幔}代表大陆岩石圈地幔的平均产物,取值6.5 Ra(Stuart et al., 1994b)。带入各个样品数据即可知,姐纳各普金矿床

幔源He占比介于0.93%~1.08%,平均为0.99%,明显低于分布在雅鲁藏布江缝合带(IYS)内的藏南典型造山型金矿床的幔源He占比(3%~17%;韦慧晓等,2010;Sun et al., 2016b),因此幔源He对姐纳各普金矿床成矿流体He的贡献可忽略不计。

在图9中,姐纳各普金矿床数据投点集中分布于壳源流体边部,靠近壳源流体,而远离幔源流体和大气饱和水区域,同样表明成矿流体中无幔源流体的混入。结合前述图8中的推论认为,姐纳各普金矿床成矿流体应以壳源变质流体为主,并有改造型大气饱和水或建造水的混合。

对于变质流体中Ar同位素组成而言,其⁴⁰Ar/³⁶Ar比值可变化于300~20 000,但多在(1~10)×10³之间,主要与壳源岩石岩性、K含量、变质作用类型、成岩/成矿年龄和构造环境等因素相关,如古老流体的⁴⁰Ar/³⁶Ar比值(2.65 Ga捕获的流体可达20 000)大于年轻流体,进变质作用相关流体的⁴⁰Ar/³⁶Ar比值大于退变质作用相关流体等(Ozima and Podosek, 1983; Torgersen, 1989; Kendrick et al., 2001, 2002a, 2002b, 2005, 2006, 2007, 2011)。姐纳各普金矿床的⁴⁰Ar/³⁶Ar比值分布较为集中分布于308.0~386.3,平均比值347.1,与扎西康矿集区内的明赛(Zhang et al., 2020)、马扎拉(张刚阳, 2012; 翟伟等, 2018)及雅鲁藏布江缝合带(IYS)内及边缘的邦布(韦慧晓等, 2010; Sun et al., 2016b)、折木朗(Zhou et al., 2014)和查拉普(张刚阳, 2012)等新生代金矿床相似(图9),介于壳源放射性Ar和大气Ar之间,但低于典型的变质流体⁴⁰Ar/³⁶Ar比值。这一现象可能的解释为姐纳各普金矿床成矿时代较新且有低⁴⁰Ar/³⁶Ar比值的改造成型大气饱和水或建造水参与成矿的缘故。根据前人提出的放射性成因的⁴⁰Ar*含量占比估算公式:⁴⁰Ar*(%)=[(⁴⁰Ar/³⁶Ar)_{样品}-295.5]/(⁴⁰Ar/³⁶Ar)_{样品}×100(Ballentine and Burnard, 2002),可计算得到姐纳各普金矿床⁴⁰Ar*占比介于4.06%~23.51%,平均为14.18%,相应的大气Ar含量变化于76.49%~95.94%,平均为85.82%;结合He同位素组成,反映出成矿流体为富集壳源He、大气Ar的建造水与富集放射成因壳源Ar的壳源流体的混合,而后者正是前面描述的壳源变质流体。同时,扎西康矿集区马扎拉金锑矿床地层黄铁矿的⁴⁰Ar*占比介于15.43%~76.69%,平均为42.85%,相应的大气Ar占比为23.31%~84.57%,平均为57.15%(翟伟等, 2018),指示经历

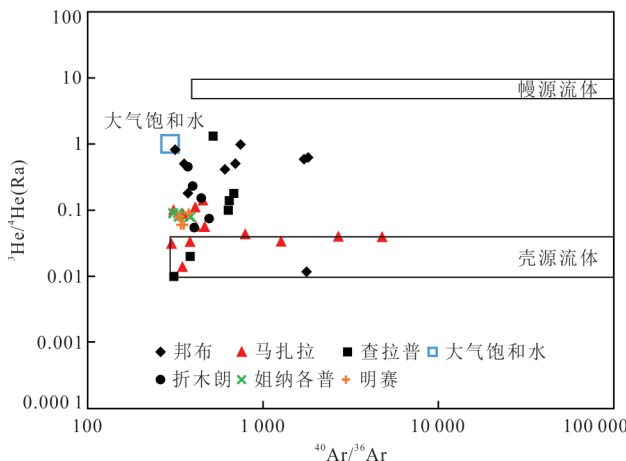
图9 姐纳各普金矿床 ${}^3\text{He}/{}^4\text{He}$ — ${}^{40}\text{Ar}/{}^{36}\text{Ar}$ 图解

Fig.9 ${}^3\text{He}/{}^4\text{He}$ — ${}^{40}\text{Ar}/{}^{36}\text{Ar}$ diagram of pyrite in Jienagepu gold deposit

壳源流体数据引自 Andrews(1985);幔源数据引自 Stuart *et al.*(1994b);其他金矿床数据源同图8

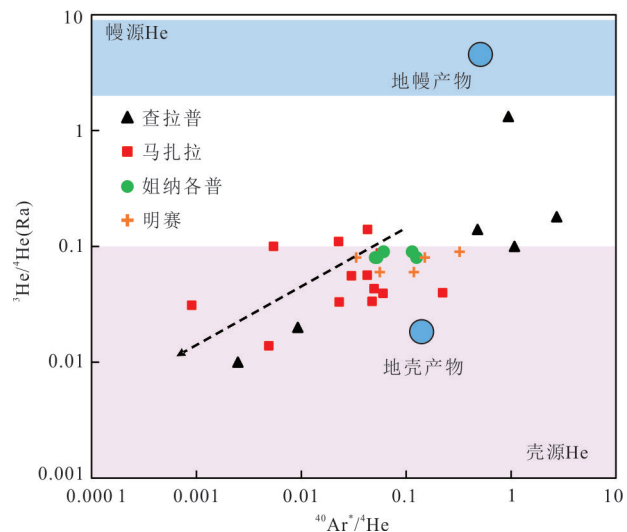
图10 姐纳各普金矿床 ${}^3\text{He}/{}^4\text{He}$ — ${}^{40}\text{Ar}^*/{}^4\text{He}$ 图解

Fig.10 ${}^3\text{He}/{}^4\text{He}$ — ${}^{40}\text{Ar}^*/{}^4\text{He}$ diagram of pyrite in Jienagepu gold deposit

壳源流体数据引自 Andrews(1985);幔源数据引自 Stuart *et al.*(1994b);其他金矿床数据源同图8

了低绿片岩相变质作用的地层黄铁矿同样经历了变质流体与建造水的相互作用。

值得一提的是,姐纳各普金矿床的 ${}^{40}\text{Ar}^*/{}^4\text{He}$ 比值介于0.050 6~0.125 2,平均比值0.080 6,低于大陆岩石圈地幔和地壳岩石的 ${}^{40}\text{Ar}^*/{}^4\text{He}$ 比值,分别为0.5和0.2(Andrews, 1985).在图10中,不同于含有幔源流体参与成矿的藏南典型造山型金矿床(韦慧晓等,2010;Sun *et al.*, 2016b),姐纳各普金矿床位于地壳产物区域,远离地幔产物区域,并且与扎西康矿集区内的马扎拉(张刚阳,2012;翟伟等,2018)和明赛金矿床(Zhang *et al.*, 2020)大致呈线性分布,具有向远低于地壳产物区域的建造水漂移的趋势(图10),指示姐纳各普金矿床的成矿流体主要为壳源变质流体,并有改造型大气饱和水或建造水的加入。

地质流体的来源大致可分为大气源、壳源和幔源3大类(Matsumoto *et al.*, 2001; Trieloff *et al.*, 2002; Buikin *et al.*, 2005; Marchesi *et al.*, 2010),但大多数热液矿床的成矿流体来源往往并不具有典型的单一来源特征,而具有混源的特点(Stuart and Turner, 1992;毛景文和李晓峰,2004;孙晓明等;2006).本次研究结果同样指示,姐纳各普金矿床成矿流体并非源于单一性质的流体,而是主要源于壳源变质流体,并有建造水的混入。

5.2 成矿物质来源

在热液金矿床中,由于Au元素的活动性极差,

并且也缺少可供追溯物源的Au的同位素,而黄铁矿、毒砂和辉锑矿等硫化物作为最重要且常见的载金硫化物,同时S又是Au的矿化剂,由此可将热液金矿床成矿物质来源问题转化为硫源问题.因此,在热液金矿床研究中,通常将载金矿物的S同位素用于间接示踪成矿物质的来源(Boyle, 1987),并且取得了良好的效果.

研究显示,当矿床矿石矿物组合中未出现硫酸盐矿物时,表明成矿流体中的S主要以HS和S²⁻的形式存在(Ohmoto, 1972; Ohmoto and Rye, 1979; Seal, 2006).野外地质调查及室内岩矿鉴定发现,姐纳各普金矿床矿石中主要矿石矿物包括黄铁矿、方铅矿、闪锌矿、毒砂、辉锑矿等,主要脉石矿物有石英、方解石、绢云母等,在矿体与围岩中均未发现重晶石、石膏等硫酸盐矿物的存在或报道,指示主成矿期成矿流体中的S主要以HS和S²⁻的形式存在.因此,本次针对姐纳各普金矿床黄铁矿的原位S同位素测试得到的数据可真实代表成矿流体的S同位素组成.

研究表明,硫化物中的硫源主要包括3种来源:(1)地幔或地壳物质经部分熔融产生的酸性岩浆熔体,其 $\delta^{34}\text{S}$ 值约为0±3‰,且呈现塔式分布的特征.酸性岩浆作用期后热液流体的 $\delta^{34}\text{S}$ 值则介于-3‰~7‰;(2)沉积硫,其 $\delta^{34}\text{S}$ 值一般为较大的负值,且变化范围大,多为生物成因;(3)海相或海

水硫,随地质历史时期的不同而变化,但 $\delta^{34}\text{S}$ 值多表现为较大的正值(约 20‰),且变化范围较小(Ohmoto, 1972; Ohmoto and Rye, 1979; Seal, 2006)。

从姐纳各普金矿床黄铁矿原位 S 同位素测试结果(表 2、图 7)可知,矿床中 17 个测点的 $\delta^{34}\text{S}$ 值分布集中,总体变化于 1‰~3‰,与雅鲁藏布江缝合带(IYS)内分布的造山型金矿床的 $\delta^{34}\text{S}$ 值(温春齐等, 2006; Jiang *et al.*, 2009; 韦慧晓等, 2010; 张刚阳, 2012; 张雄, 2017)接近(图 11);2 件地层黄铁矿样品的 $\delta^{34}\text{S}$ 值分别为 14.46‰ 和 14.79‰,与同时代海水硫酸的 $\delta^{34}\text{S}$ 值(16.8‰~19.1‰; Kampschulte and Strauss, 2004)相当。这一测试结果在排除成矿物质源于海相硫的同时,也直观指示成矿物质来源较为单一,主要为幔源。然而,从已有的研究成果来看,目前的勘查及研究工作并未在矿集区及区域上发现或报道有明显的中新世甚至新生代幔源岩浆活动的证据,尽管藏南地区广布的辉绿岩、英安岩和流纹岩等被认为与 Kerguelen 地幔柱活动相关(Zhu *et al.*, 2011),但其活动时代(132 Ma; Zhu *et al.*, 2009)明显早于姐纳各普金矿床成矿年龄(17.6±1.8 Ma; 董随亮等, 2017),这表明成矿物质直接来源于地幔的可能性较小。

前人研究显示,热液金矿床的 $\delta^{34}\text{S}$ 值差别很大,其中太古宙金矿床硫同位素 $\delta^{34}\text{S}$ 值变化在 0‰~9‰(Kerrick, 1987, 1989),而显生宙金矿床则变化范围更大, $\delta^{34}\text{S}$ 值介于 -20‰~25‰(Peters and Golding,

1989; Kontak *et al.*, 1990),暗示其没有统一的硫源(McCuaig *et al.*, 1998; Tomkins and Grundy, 2009),如刘伟等(2002)报道了东天山金窝子金矿床的 $\delta^{34}\text{S}$ 值介于 -5‰~5‰,认为成矿物质来源于地幔至地壳之间的各种储库;王团华等(2009)综合分析了豫西小秦岭—熊耳地区的 11 个金矿床的 S 同位素组成,发现其 $\delta^{34}\text{S}$ 值亦介于 -5‰~5‰,并认为矿床成矿物质来源于造山带环境下壳幔相互作用过程中的相关地质单元或地质体,属于壳幔物质均一化的深源;陈翠华等(2014)报道了云南老寨湾金矿床的 $\delta^{34}\text{S}$ 值介于 -3.0‰~7.8‰,认为成矿物质来源于上地壳;李杰等(2016)对岗岔金矿床的研究发现其 $\delta^{34}\text{S}$ 值介于 0.6‰~1.3‰,认为成矿物质主要为壳幔混源,但以深部幔源为主;孙琦等(2016)对砂宝斯金矿床的研究发现其 $\delta^{34}\text{S}$ 值介于 0.2‰~5.6‰,结合 Pb 同位素组成认为成矿物质主要为壳幔混源;商青青等(2017)报道了延边杨金沟造山型金矿床的 $\delta^{34}\text{S}$ 值介于 0.6‰~2.7‰,认为矿床金属物质源于上地幔;丁辉等(2018)对东准噶尔绿源金矿床的研究发现其 $\delta^{34}\text{S}$ 值介于 0.2‰~2.8‰,认为成矿物质具有壳幔混源的特点;裴英茹等(2016)对藏北商旭造山型金矿床的研究发现其 $\delta^{34}\text{S}$ 值介于 -4.5‰~1.0‰,显示成矿物质源于上地壳,并有造山带内混杂岩的贡献;对于扎西康矿集区北侧雅鲁藏布江缝合带(IYS)内的典型造山型金矿床(图 11)而言,念扎金矿床 $\delta^{34}\text{S}$ 值介于 -2.9‰~1.9‰,暗示成矿物质

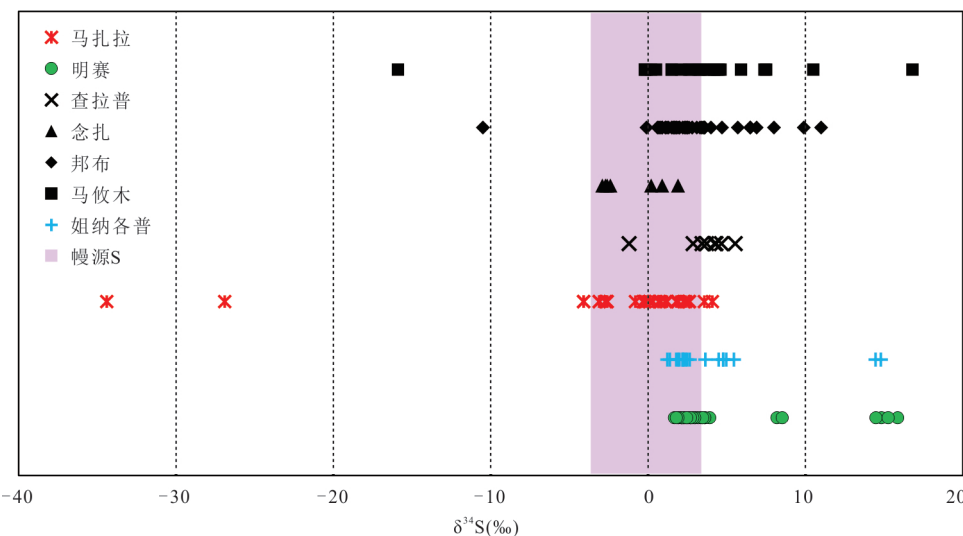


图 11 姐纳各普金矿床 S 同位素组成

Fig.11 S isotopic compositions of the Jienagepu gold deposit

马扎拉数据引自杨竹森等(2006)、戚学祥等(2008)、张刚阳(2012)、梁维(2014)和谢玉玲等(2019);明赛数据引自卢柳(2019);查拉普数据引自张刚阳(2012);念扎数据引自张雄(2017);邦布数据引自韦慧晓等(2010);马攸木数据引自温春齐等(2006)和 Jiang *et al.*(2009)

源于地幔(张雄,2017);邦布金矿床 $\delta^{34}\text{S}$ 值介于 $1.2\text{\textperthousand} \sim 3.6\text{\textperthousand}$,表明成矿物质主要源于朗杰学增生楔(韦慧晓等,2010;Sun *et al.*,2016b);马攸木金矿床 $\delta^{34}\text{S}$ 值介于 $-0.2\text{\textperthousand} \sim 4.5\text{\textperthousand}$,推测成矿物质源于震旦系(Z)一寒武系(C)齐吾贡巴群变质碎屑岩系(温春齐等,2006;Jiang *et al.*,2009).Cao *et al.*(2020)报道了扎西康矿集区东部措美县的Laqiong造山型金矿床的 $\delta^{34}\text{S}$ 值介于 $-1.1\text{\textperthousand} \sim 2.3\text{\textperthousand}$,结合Pb同位素组成认为成矿物质来源于加厚的大陆地壳.这些研究表明,尽管处于同一成矿带上、且具相似 $\delta^{34}\text{S}$ 值的同类型金矿床,其成矿物质来源仍差异较大,并没有统一的硫源.

综合对比前人研究成果,结合姐纳各普金矿床 $\delta^{34}\text{S}$ 值与幔源S接近且分布集中的特点,本次研究认为姐纳各普金矿床成矿物质主要来自地壳深部壳幔物质均一化的深源,即地壳和地幔之间经历了充分的物质和能量交换相互作用形成的较为均一的地质体(丁辉等,2018;赵子福等,2021).

5.3 矿床成因

由于热液矿床的成矿过程受地层、构造、岩浆等多种地质因素的共同制约,其产出形式也多种多样,导致其成因分类的思路和依据也难以统一(李洪梁和李光明,2019),因而分类方案较多,如按照成矿地质作用的性质(朱奉三,1982)、赋矿围岩性质(涂光炽,1986)、控制矿床定位的地质因素(陈衍景等,1992)、矿床产出的构造地质背景(Kerrich *et al.*,2000)和主导成矿系统发育的地质作用特征(陈衍景等,2007)等分类方案.考虑到不同分类方案在文献中的使用频率和成矿流体性质及来源的差异性,本文采用陈衍景等(2007)依据主导成矿系统发育的地质作用特征将其分为造山型、浆控高温热液型、浅成低温热液型和卡林型4类.该分类方案认为,造山型金矿床成矿流体来源于变质流体,具有低盐度、富CO₂的特点;浆控高温热液型矿床成矿流体来源于高温、高盐度、富CO₂的岩浆热液;浅成低温热液型金矿床成矿流体主要来自岩浆活动驱动的建造水,并有岩浆热液的加入;卡林型金矿床成矿流体则主要源自低温、低盐度的浅成建造水(陈衍景等,2007).

本次研究发现,姐纳各普金矿床矿体受断裂及层间破碎带控制,赋矿岩石为破碎带中的蚀变凝灰岩,矿石组构多见块状、角砾状、网脉状、晶洞及晶簇构造和结晶、交代结构,主要矿石矿物包括自然

金、方铅矿、闪锌矿、辉锑矿、辰砂、黄铁矿、毒砂及少量磁铁矿,脉石矿物主要为石英、绢云母和方解石.围岩蚀变主要发育硅化、黄铁矿化、绢云母化和方解石化.主成矿阶段黄铁矿流体包裹体⁴He含量介于 $0.038 \times 10^{-7} \sim 0.446 \times 10^{-7} \text{ cm}^3 \text{ STP/g}$,平均含量 $0.200 \times 10^{-7} \text{ cm}^3 \text{ STP/g}$; ³He/⁴He比值介于0.08~0.09 Ra,平均比值约为0.08 Ra;⁴⁰Ar含量变化于 $0.049 \times 10^{-7} \sim 0.132 \times 10^{-7} \text{ cm}^3 \text{ STP/g}$,平均含量 $0.084 \times 10^{-7} \text{ cm}^3 \text{ STP/g}$;⁴⁰Ar/³⁶Ar比值介于308.0~386.3,平均比值347.1,显示成矿流体主要源于壳源变质流体,并有建造水的混入.黄铁矿 $\delta^{34}\text{S}$ 值分布集中,主体变化于 $1\text{\textperthousand} \sim 3\text{\textperthousand}$,平均值为 $2.98\text{\textperthousand}$,指示成矿物质为壳幔物质均一化的深源.同时,李洪梁等(2017)对矿床探槽中含金石英脉中石英流体包裹体的研究显示,矿床成矿流体属于中低温、低盐度、低密度、富CO₂的H₂O-NaCl-CO₂-CH₄-N₂体系.这些特征与雅鲁藏布江缝合带(IYS)(温春齐等,2006;Jiang *et al.*,2009;韦慧晓等,2010;Sun *et al.*,2016b;张雄,2017;王庆飞等,2019,2020)及世界典型造山型金矿床(Goldfarb *et al.*,2001;Groves *et al.*,2003,2005,2020;Goldfarb and Groves,2015;Groves and Santosh,2015)极为相似.由此,作者认为姐纳各普金矿床属于造山型金矿床.

5.4 地质意义

目前,对于喜马拉雅带造山型金矿床的研究,传统观点多认为其主要发育在雅鲁藏布江缝合带(IYS)内及两侧的脆一韧性断层中,形成于主碰撞造山(65~41 Ma;侯增谦等,2006c)挤压构造环境,与典型造山型金矿床形成于同造山环境的观点极为吻合(Goldfarb *et al.*,2001;Groves *et al.*,2003,2005,2020;陈衍景等,2007),如温春齐等(2004)利用马攸木金矿床主成矿阶段内的绢云母Ar-Ar定年获得了44 Ma的成矿年龄,认为其形成于印度—欧亚大陆碰撞造山的主碰撞阶段;念扎金矿床绢云母Ar-Ar定年显示,成矿时代为43.6 Ma,属于主碰撞造山阶段的产物(张雄,2017);Sun *et al.*(2016b)通过绢云母Ar-Ar定年分别得到了44.8 Ma和49.5 Ma的成矿年龄,指示邦布造山型金矿床形成于印度—欧亚大陆碰撞造山的主碰撞造山阶段.正因如此,多数研究者的目光也主要集中于雅鲁藏布江缝合带(IYS)及两侧,而忽略了特提斯喜马拉雅构造带(TH)内分布的众多金矿床(点).

针对特提斯喜马拉雅构造带(TH)东段藏南铅

锌金锑成矿带中金矿床成因的研究,由于受印度—欧亚大陆碰撞造山作用的影响,矿床的分带和成矿时代跨度范围较大,即从北向南出现了金→金锑→铅锌矿床的分带性,成矿时代从古近纪到新近纪均有涵盖,因此曾有不同学者提出过差别迥异的观点。郑有业等(2004)通过典型矿床地质特征对比,指出查拉普金矿床应属于卡林型金矿床,并提出带内还可能存在浅成低温热液型矿床;侯增谦等(2006b)、戚学祥等(2008)和 Hou and Cook(2009)等学者通过对印度—欧亚大陆碰撞造山过程阶段的划分,细致介绍了各造山阶段内产出的不同类型热液矿床,综合对比分析认为雅鲁藏布江缝合带(IYS)存在一条富有巨大远景的金矿化带,矿床成因属造山型金矿床;韦慧晓等(2010)、Sun *et al.*(2016b)、张雄(2017)和王庆飞等(2019, 2020)学者对雅鲁藏布江缝合带(IYS)内的金矿床进行了系统的矿床地质与地球化学特征研究发现,这些金矿床矿体严格受脆—韧性断裂控制,成矿流体为来源于变质流体的富 CO₂ 的中—低温、低盐度、低密度的 H₂O-NaCl-CO₂-CH₄-N₂ 体系,并有幔源流体的加入,成矿物质主要来源于深部地幔、围岩地层或相关变质岩系等;与全球典型造山型金矿床的综合对比认为,这些金矿床属于与印度—欧亚大陆碰撞造山作用密切相关的典型造山型金矿床。对于扎西康矿集区内的金成矿作用,李洪梁(2020)在前人研究成果基础上,结合多源同位素分析认为,马扎拉金矿床为造山型金矿床;Zhang *et al.*(2020)对明赛金矿床的系统研究发现,矿床成矿流体属于壳源变质流体或与地幔去气有关,具有低温、低盐度、低密度富 CO₂ 的特点,成矿物质为深源,属较为典型的造山型金矿床。

对于姐纳各普金矿床成矿时代,董随亮等(2017)利用含金石英脉中的绢云母进行了 Ar-Ar 定年,将其限定在 17.6±1.8 Ma,为中新世,形成于后碰撞伸展构造背景(<25 Ma; 侯增谦等, 2006a);而在姐纳各普金矿床南侧的明赛金矿床(图 2),与金矿化密切相关绢云母 Ar-Ar 定年获得了 16.03±0.31 Ma 的成矿年龄(Zhang *et al.*, 2020);至于矿集区西北侧的马扎拉金矿床,尽管其发现时间较早,但由于缺少合适的定年矿物,至今尚未能直接限定其成矿时代,不过张建芳等(2011)通过对穿切金矿体岩体的研究,将其成矿时代限定在了中新世。最近,在扎西康矿集区西侧的措美县 Laqiong 地区,

Cao *et al.*(2020)也报道了还存在 14 Ma 的金矿化作用。通过对对比发现,这些金矿床均形成于中新世,属后碰撞伸展构造背景下的产物,矿体受伸展构造控制,成矿流体具有中低温、低盐度、低密度、富 CO₂ 的特点,成矿流体(壳源变质流体)及物质来源(深源)相似,暗示喜马拉雅带中新世金矿化作用较为普遍,且具有相当规模。

综上所述,作者认为喜马拉雅带自印度—欧亚大陆碰撞造山以来,至少存在 2 期造山型金成矿作用,第一期为始新世,形成于主碰撞造山(65~41 Ma; 侯增谦等, 2006c)挤压构造环境,以雅鲁藏布江缝合带(IYS)内邦布、马攸木、念扎等金矿床为代表;第二期为中新世,形成于后碰撞(<25 Ma; 侯增谦等, 2006a)伸展构造背景,以扎西康矿集区新近发现的姐纳各普和明赛等金矿床为代表。可见,作为印度—欧亚大陆碰撞造山作用的产物,姐纳各普金矿床的发现为丰富和完善大陆碰撞造山成矿作用理论研究提供了实例,也为特提斯喜马拉雅铅锌金锑多金属成矿带寻找中新世造山型金矿床提供了找矿新方向。

6 结论

(1) 姐纳各普金矿床矿体呈层状或似层状分布,严格受伸展断裂构造控制,具蚀变岩型和石英脉型 2 种矿石。矿石组构多见块状、角砾状、网脉状、晶洞及晶簇构造和结晶、交代结构,主要矿石矿物包括自然金、方铅矿、闪锌矿、辉锑矿、辰砂、黄铁矿、毒砂及少量的磁铁矿,脉石矿物主要为石英、绢云母和方解石。围岩蚀变主要发育硅化、黄铁矿化、绢云母化和方解石化。

(2) 姐纳各普金矿床黄铁矿流体包裹体内 ⁴He 含量介于 0.038×10^{-7} ~ $0.446 \times 10^{-7} \text{ cm}^3 \text{ STP/g}$, 平均含量 $0.200 \times 10^{-7} \text{ cm}^3 \text{ STP/g}$; ³He/⁴He 比值介于 0.08~0.09 Ra, 平均比值约为 0.08 Ra; ⁴⁰Ar 含量变化于 0.049×10^{-7} ~ $0.132 \times 10^{-7} \text{ cm}^3 \text{ STP/g}$, 平均含量 $0.084 \times 10^{-7} \text{ cm}^3 \text{ STP/g}$; ⁴⁰Ar/³⁶Ar 比值介于 308.0~386.3, 平均比值 347.1; ³⁸Ar/³⁶Ar 比值介于 0.188 5~0.189 3, 平均比值 0.188 9, 显示成矿流体主要源于壳源变质流体,并有建造水的混入。黄铁矿 δ³⁴S 值分布集中,主体变化于 1‰~3‰, 平均为 2.98‰, 指示成矿物质来自地壳深部壳幔物质均一化的深源。

(3) 综合对比已有研究成果认为,姐纳各普金

矿床为形成于中新世的造山型金矿床,其成因的厘定表明,喜马拉雅带自印度—欧亚大陆碰撞造山以来,发育始新世和中新世2期造山型金成矿作用,这对丰富和完善大陆碰撞成矿理论及区域找矿勘查具有重要意义。

References

- Adam, M.M.A., Lv, X., Abdel Rahman, A.A., et al., 2020. In-Situ Sulfur Isotope and Trace Element Compositions of Pyrite from the Neoproterozoic Haweit Gold Deposit, NE Sudan: Implications for the Origin and Source of the Sulfur. *Ore Geology Reviews*, 120: 103405. <https://doi.org/10.1016/j.oregeorev.2020.103405>
- Andrews, J.N., 1985. The Isotopic Composition of Radiogenic Helium and Its Use to Study Groundwater Movement in Confined Aquifers. *Chemical Geology*, 49(1–3): 339–351. [https://doi.org/10.1016/0009-2541\(85\)90166-4](https://doi.org/10.1016/0009-2541(85)90166-4)
- Ballentine, C.J., Burnard, P.G., 2002. Production, Release and Transport of Noble Gases in the Continental Crust. *Reviews in Mineralogy and Geochemistry*, 47(1): 481–538. <https://doi.org/10.2138/rmg.2002.47.12>
- Bao, Z.A., Chen, L., Zong, C.L., et al., 2017. Development of Pressed Sulfide Powder Tablets for In Situ Sulfur and Lead Isotope Measurement Using LA-MC-ICP-MS. *International Journal of Mass Spectrometry*, 421: 255–262. <https://doi.org/10.1016/j.ijms.2017.07.015>
- Boyle, R.W., 1987. Gold: History and Genesis of Deposits. Van Nostrand Reinhold, New York.
- Buikin, A., Trieloff, M., Hopp, J., et al., 2005. Noble Gas Isotopes Suggest Deep Mantle Plume Source of Late Cenozoic Mafic Alkaline Volcanism in Europe. *Earth and Planetary Science Letters*, 230(1–2): 143–162. <https://doi.org/10.1016/j.epsl.2004.11.001>
- Burnard, P.G., Hu, R., Turner, G., et al., 1999. Mantle, Crustal and Atmospheric Noble Gases in Ailaoshan Gold Deposits, Yunnan Province, China. *Geochimica et Cosmochimica Acta*, 63(10): 1595–1604. [https://doi.org/10.1016/s0016-7037\(99\)00108-8](https://doi.org/10.1016/s0016-7037(99)00108-8)
- Burnard, P.G., Polya, D.A., 2004. Importance of Mantle Derived Fluids during Granite Associated Hydrothermal Circulation: He and Ar Isotopes of Ore Minerals from Panasqueira. *Geochimica et Cosmochimica Acta*, 68(7): 1607–1615. <https://doi.org/10.1016/j.gca.2003.10.008>
- Cao, H. W., Li, G. M., Zhang, Z., et al., 2020. Miocene Sn Polymetallic Mineralization in the Tethyan Himalaya, Southeastern Tibet: A Case Study of the Cuonadong Deposit. *Ore Geology Reviews*, 119: 103403. <https://doi.org/10.1016/j.oregeorev.2020.103403>
- Chen, C.H., Zhao, D.K., Gu, X.X., et al., 2014. Discussion on Ore-Forming Material Sources of the Laozhaiwan Gold Deposit, Yunnan. *Bulletin of Mineralogy, Petrology and Geochemistry*, 33(1): 23–30 (in Chinese with English abstract).
- Chen, L., Chen, K. Y., Bao, Z. A., et al., 2017. Preparation of Standards for In Situ Sulfur Isotope Measurement in Sulfides Using Femtosecond Laser Ablation MC-ICP-MS. *Journal of Analytical Atomic Spectrometry*, 32(1): 107–116. <https://doi.org/10.1039/c6ja00270f>
- Chen, Y. J., Fu, S. G., Lu, B., et al., 1992. Classification of Metallogenic Series and Types of Gold Deposits. *Advance in Earth Sciences*, 7(3): 73–79 (in Chinese with English abstract).
- Chen, Y. J., Ni, P., Fan, H. R., et al., 2007. Diagnostic Fluid Inclusions of Different Types Hydrothermal Gold Deposits. *Acta Petrologica Sinica*, 23(9): 2085–2108 (in Chinese with English abstract).
- Ding, H., Ge, W. S., Dong, L. H., et al., 2018. Geological Characteristics and Gold Source Analysis of the Luyuan Gold Deposit in Eastern Junggar, Xinjiang. *Acta Geologica Sinica*, 92(5): 1019–1040 (in Chinese with English abstract).
- Dong, S. L., Huang, Y., Li, G. M., et al., 2017. Geology and Mineralization Dating of Jienagepu Gold Deposit in Southern Tibet with Implication from Zhaxikang Pb-Zn-Au-Sb Metallogenic System. *Resources and Industries*, 19(5): 56–64 (in Chinese with English abstract).
- Duan, J. L., Tang, J. X., Lin, B., 2016. Zinc and Lead Isotope Signatures of the Zhaxikang Pb-Zn Deposit, South Tibet: Implications for the Source of the Ore-Forming Metals. *Ore Geology Reviews*, 78: 58–68. <https://doi.org/10.1016/j.oregeorev.2016.03.019>
- Faure, K., 2003. δ D Values of Fluid Inclusion Water in Quartz and Calcite Ejecta from Active Geothermal Systems: Do Values Reflect Those of Original Hydrothermal Water? *Economic Geology*, 98(3): 657–660. <https://doi.org/10.2113/gsecongeo.98.3.657>
- Fu, J. G., Li, G. M., Wang, G. H., et al., 2017. First Field Identification of the Cuonadong Dome in Southern Tibet: Implications for EW Extension of the North Himalayan Gneiss Dome. *International Journal of Earth Sciences*, 106(5): 1581–1596. <https://doi.org/10.1007/s00531-016-1368-2>
- Fu, J. G., Li, G. M., Wang, G. H., et al., 2018. Establishment of the North Himalayan Double Gneiss Domes: Evidence from Field Identification of the Cuonadong Dome, South

- Tibet. *Geology in China*, 45(4): 783—802(in Chinese with English abstract).
- Goldfarb, R.J., Groves, D.I., 2015. Orogenic Gold: Common or Evolving Fluid and Metal Sources through Time. *Lithos*, 233:2—26. <https://doi.org/10.1016/j.lithos.2015.07.011>
- Goldfarb, R.J., Groves, D.I., Gardoll, S., 2001. Orogenic Gold and Geologic Time: A Global Synthesis. *Ore Geology Reviews*, 18(1—2): 1—75. [https://doi.org/10.1016/s0169-1368\(01\)00016-6](https://doi.org/10.1016/s0169-1368(01)00016-6)
- Grant, K., Gleeson, S.A., Roberts, S., 2003. The High-Temperature Behavior of Defect Hydrogen Species in Quartz: Implications for Hydrogen Isotope Studies. *American Mineralogist*, 88(2—3): 262—270. <https://doi.org/10.2138/am-2003-2-302>
- Groves, D.I., Condie, K.C., Goldfarb, R.J., et al., 2005. 100th Anniversary Special Paper: Secular Changes in Global Tectonic Processes and Their Influence on the Temporal Distribution of Gold-Bearing Mineral Deposits. *Economic Geology*, 100(2): 203—224. <https://doi.org/10.2113/gsecongeo.100.2.203>
- Groves, D.I., Goldfarb, R.J., Robert, F., et al., 2003. Gold Deposits in Metamorphic Belts: Overview of Current Understanding, Outstanding Problems, Future Research, and Exploration Significance. *Economic Geology*, 98(1): 1—29. <https://doi.org/10.2113/gsecongeo.98.1.1>
- Groves, D.I., Santosh, M., 2015. Province-Scale Commonalities of Some World-Class Gold Deposits: Implications for Mineral Exploration. *Geoscience Frontiers*, 6(3): 389—399. <https://doi.org/10.1016/j.gsf.2014.12.007>
- Groves, D.I., Santosh, M., Zhang, L., 2020. A Scale-Integrated Exploration Model for Orogenic Gold Deposits Based on a Mineral System Approach. *Geoscience Frontiers*, 11(3): 719—738. <https://doi.org/10.1016/j.gsf.2019.12.007>
- Guo, C.Y., Zhang, W.Z., Ge, L.S., et al., 2011. Several Questions on Tracing Ore Forming Fluid by Using Hydrogen and Oxygen Isotope System. *Journal of Mineralogy and Petrology*, 31(3): 41—47(in Chinese with English abstract).
- Hoefs, J., 1997. Stable Isotope Geochemistry. Springer-Verlag, Berlin. <https://doi.org/10.1007/978-3-662-03377-7>
- Hou, Z.Q., Cook, N.J., 2009. Metallogenesis of the Tibetan Collisional Orogen: A Review and Introduction to the Special Issue. *Ore Geology Reviews*, 36(1—3): 2—24. <https://doi.org/10.1016/j.oregeorev.2009.05.001>
- Hou, Z.Q., Mo, X.X., Yang, Z.M., et al., 2006b. Metallogenesis in the Collisional Orogen of the Qinghai-Tibet Plateau: Tectonic Setting, Tempo-Spatial Distribution and Ore Deposit Types. *Geology in China*, 33(2): 340—351 (in Chinese with English abstract).
- Hou, Z.Q., Qu, X.M., Yang, Z.S., et al., 2006a. Metallogenesis in Tibetan Collisional Orogenic Belt: III. Mineralization in Post-Collisional Extension Setting. *Mineral Deposits*, 25(6): 629—651(in Chinese with English abstract).
- Hou, Z.Q., Wang, E.Q., 2008. Metallogenesis of the Indo-Asian Collisional Orogen: New Advances. *Acta Geoscientifica Sinica*, 29(3): 275—292(in Chinese with English abstract).
- Hou, Z.Q., Yang, Z.S., Xu, W.Y., et al., 2006c. Metallogenesis in Tibetan Collisional Orogenic Belt: I. Mineralization in Main Collisional Orogenic Setting. *Mineral Deposits*, 25(4): 337—358(in Chinese with English abstract).
- Hu, R.Z., 1997. Isotope Geochemistry of Helium and Argon in Ore-Forming Fluids. *Bulletin of Mineralogy, Petrology and Geochemistry*, 16(2): 52—56(in Chinese with English abstract).
- Hu, R.Z., Burnard, P.G., Bi, X.W., et al., 2009. Mantle-Derived Gaseous Components in Ore-Forming Fluids of the Xiangshan Uranium Deposit, Jiangxi Province, China: Evidence from He, Ar and C Isotopes. *Chemical Geology*, 266(1—2): 86—95. <https://doi.org/10.1016/j.chemgeo.2008.07.017>
- Hu, R.Z., Burnard, P.G., Turner, G., et al., 1998. Helium and Argon Isotope Systematics in Fluid Inclusions of Machangqing Copper Deposit in West Yunnan Province, China. *Chemical Geology*, 146(1—2): 55—63. [https://doi.org/10.1016/s0009-2541\(98\)00003-5](https://doi.org/10.1016/s0009-2541(98)00003-5)
- Huang, C.M., Li, G.M., Zhang, Z., et al., 2018. Petrogenesis of the Cuonadong Leucogranite in South Tibet: Constraints from Bulk-Rock Geochemistry and Zircon U-Pb Dating. *Earth Science Frontiers*, 25(6): 182—195(in Chinese with English abstract).
- Jiang, S.H., Nie, F.J., Hu, P., et al., 2009. Mayum: An Orogenic Gold Deposit in Tibet, China. *Ore Geology Reviews*, 36(1—3): 160—173. <https://doi.org/10.1016/j.oregeorev.2009.03.006>
- Kampschulte, A., Strauss, H., 2004. The Sulfur Isotopic Evolution of Phanerozoic Seawater Based on the Analysis of Structurally Substituted Sulfate in Carbonates. *Chemical Geology*, 204(3—4): 255—286. <https://doi.org/10.1016/j.chemgeo.2003.11.013>
- Kendrick, M.A., Baker, T., Fu, B., et al., 2008. Noble Gas and Halogen Constraints on Regionally Extensive Mid-Crustal Na-Ca Metasomatism, the Proterozoic Eastern Mount Isa Block, Australia. *Precambrian Research*, 163(1—2): 131—150. <https://doi.org/10.1016/j.precamres.2007.08.015>

- Kendrick, M.A., Burgess, R., Harrison, D., et al., 2005. Noble Gas and Halogen Evidence for the Origin of Scandinavian Sandstone-Hosted Pb-Zn Deposits. *Geochimica et Cosmochimica Acta*, 69(1): 109–129. <https://doi.org/10.1016/j.gca.2004.05.045>
- Kendrick, M. A., Burgess, R., Pattrick, R. A. D., et al., 2001. Fluid Inclusion Noble Gas and Halogen Evidence on the Origin of Cu-Porphyry Mineralising Fluids. *Geochimica et Cosmochimica Acta*, 65(16):2651–2668.
- Kendrick, M.A., Burgess, R., Pattrick, R.A.D., et al., 2002a. Hydrothermal Fluid Origins in a Fluorite-Rich Mississippi Valley-Type District: Combined Noble Gas (He, Ar, Kr) and Halogen (Cl, Br, I) Analysis of Fluid Inclusions from the South Pennine Ore Field, United Kingdom. *Economic Geology*, 97(3): 435–451. <https://doi.org/10.2113/gsecongeo.97.3.435>
- Kendrick, M.A., Burgess, R., Leach, D., et al., 2002b. Hydrothermal Fluid Origins in Mississippi Valley-Type Ore Districts: Combined Noble Gas (He, Ar, Kr) and Halogen (Cl, Br, I) Analysis of Fluid Inclusions from the Illinois-Kentucky Fluorspar District, Viburnum Trend, and Tri-State Districts, Midcontinent United States. *Economic Geology*, 97(3):453–469. <https://doi.org/10.2113/gsecongeo.97.3.453>.
- Kendrick, M. A., Burnard, P., 2013. Noble Gases and Halogens in Fluid Inclusions: A Journey through the Earth's Crust. *The Noble Gases as Geochemical Tracers*, 319–369. https://doi.org/10.1007/978-3-642-28836-4_11
- Kendrick, M. A., Duncan, R., Phillips, D., 2006. Noble Gas and Halogen Constraints on Mineralizing Fluids of Metamorphic versus Surficial Origin: Mt Isa, Australia. *Chemical Geology*, 235(3–4): 325–351. <https://doi.org/10.1016/j.chemgeo.2006.08.002>
- Kendrick, M. A., Honda, M., Walshe, J., et al., 2011. Fluid Sources and the Role of Abiogenic - CH₄ in Archean Gold Mineralization: Constraints from Noble Gases and Halogens. *Precambrian Research*, 189(3–4): 313–327. <https://doi.org/10.1016/j.precamres.2011.07.015>
- Kendrick, M.A., Mark, G., Phillips, D., 2007. Mid-Crustal Fluid Mixing in a Proterozoic Fe Oxide-Cu-Au Deposit, Ernest Henry, Australia: Evidence from Ar, Kr, Xe, Cl, Br, and I. *Earth and Planetary Science Letters*, 256(3–4): 328–343. <https://doi.org/10.1016/j.epsl.2006.12.032>.
- Kerrick, R., 1987. The Stable Isotope Geochemistry of Au-Ag Vein in Deposits in Metamorphic Rocks. In: Kyser, T.K., ed., *Stable Isotope Geochemistry of Low Temperature Fluids*. Mineralogical Association of Canada, 287–336.
- Kerrick, R., 1989. Lithophile Element Systematics of Gold Vein Deposits in Archean Greenstone Belts: Implications for Source Processes. *Economic Geology Monograph*, 6: 508–519.
- Kerrick, R., Goldfarb, R., Groves, D., et al., 2000. The Characteristics, Origins, and Geodynamic Settings of Supergiant Gold Metallogenic Provinces. *Science in China: Earth Sciences*, 43(1): 1–68. <https://doi.org/10.1007/bf02911933>
- Kontak, D.J., Smith, P.K., Kerrich, R., et al., 1990. Integrated Model for Meguma Group Lode Gold Deposits, Nova Scotia, Canada. *Geology*, 18(3):238–242.
- Kurz, M.D., 1986. In Situ Production of Terrestrial Cosmogenic Helium and Some Applications to Geochronology. *Geochimica et Cosmochimica Acta*, 50(12):2855–2862. [https://doi.org/10.1016/0016-7037\(86\)90232-2](https://doi.org/10.1016/0016-7037(86)90232-2)
- Li, G.M., Zhang, L.K., Jiao, Y.J., et al., 2017. First Discovery and Implications of Cuonadong Superlarge Be-W-Sn Polymetallic Deposit in Himalayan Metallogenic Belt, Southern Tibet. *Mineral Deposits*, 36(4): 1003–1008(in Chinese with English abstract).
- Li, H.L., 2016. Tectonic Setting and Genesis of the Jienagepu Gold Deposit in Zhaxikang Ore Concentration District, Tibet (Dissertation). Chengdu University of Technology, Chengdu(in Chinese with English abstract).
- Li, H. L., 2020. Metallogenesis of Orogenic Gold Deposits in Zhaxikang Ore Concentrated Area, Eastern Tethys Himalaya Belt (Dissertation). Chengdu University of Technology, Chengdu(in Chinese with English abstract)
- Li, H.L., Li, G.M., 2019. Compositional Characteristics of Pyrite Ore Formed in the Main Metallogenic Period of Various Types of Hydrothermal Gold Deposits. *Earth Science Frontiers*, 26(3): 202–210(in Chinese with English abstract).
- Li, H.L., Li, G.M., Ding, J., et al., 2020. Genesis of Zhaxikang Pb-Zn Polymetallic Deposit in Southern Tibet: Evidence from In Situ S Isotopes of Sulfides. *Journal of Jilin University (Earth Science Edition)*, 50(5): 1289–1303(in Chinese with English abstract).
- Li, H.L., Li, G.M., Li, Y.X., et al., 2017. A Study on Ore Geological Characteristics and Fluid Inclusions of Jienagepu Gold Deposit in Zhaxikang Ore Concentration District, Southern Tibet, China. *Acta Mineralogica Sinica*, 37(6): 684–696(in Chinese with English abstract).
- Li, H. L., Li, G. M., Zhang, Z., et al., 2016. Ore-Controlling Factors and Prospecting Prediction of Zhaxikang Pb-Zn Polymetallic Deposit, Southern Tibet. *Metal Mine*, (10): 103–108(in Chinese with English abstract).
- Li, J., Shen, J. F., Li, J. C., et al., 2016. Stable Isotope Geo-

- chemical Characteristics and Ore-Forming Material Source of the Gangcha Gold Deposit, Gansu Province, China. *Bulletin of Mineralogy, Petrology and Geochemistry*, 35(5):976—983(in Chinese with English abstract).
- Liang, J.L., Li, J., Liu, X.M., et al., 2020. Multiple Element Mapping and In-Situ S Isotopes of Au-Carrying Pyrite of Shuiyindong Gold Deposit, Southwestern China Using NanoSIMS: Constraints on Au Sources, Ore Fluids, and Mineralization Processes. *Ore Geology Reviews*, 123: 103576. <https://doi.org/10.1016/j.oregeorev.2020.103576>
- Liang, W., 2014. Metallogenesis of Au-Sb-Pb-Zn Mineralization in Tethys Himalaya Belt, South Tibet, China (Dissertation). China University of Geosciences, Beijing(in Chinese with English abstract).
- Liang, W., Zheng, Y.C., 2019. Hydrothermal Sericite Ar-Ar Dating of Jisong Pb-Zn Deposit, Southern Tibet. *Geology in China*, 46(1):126—139(in Chinese with English abstract).
- Liu, W., Li, J.X., Deng, J., 2002. The Source of Metallogenic Fluid and Metallogenic Material of Jinwozi Quartz Vein Gold Deposit in East Tianshan. *Science in China: Earth Sciences*, 32(Suppl.1):105—119(in Chinese).
- Lu, H.Z., 2008. Role of CO₂ Fluid in the Formation of Gold Deposits: Fluid Inclusion Evidences. *Geochimica*, 37(4): 321—328(in Chinese with English abstract).
- Lu, H.Z., Chi, G.X., Zhu, X.Q., et al., 2018. Geological Characteristics and Ore Forming Fluids of Orogenic Gold Deposits. *Geotectonica et Metallogenia*, 42(2): 244—265(in Chinese with English abstract).
- Lu, L., 2019. Geological Characteristics and Genesis of Mingsai Gold Deposit in Longzi County, Tibet (Dissertation). Chengdu University of Technology, Chengdu(in Chinese with English abstract).
- Mamyrin, B.A., Tolstikhin, I.N., 1984. Helium Isotopes in Nature. Elsevier, Amsterdam.
- Mao, J.W., Li, X.F., 2004. Mantle-Derived Fluids in Relation to Ore-Forming and Oil-Forming Processes. *Mineral Deposits*, 23(4):520—532(in Chinese with English abstract).
- Marchesi, C., Griffin, W.L., Garrido, C.J., et al., 2010. Persistence of Mantle Lithospheric Re-Os Signature during As-thenospherization of the Subcontinental Lithospheric Mantle: Insights from In Situ Isotopic Analysis of Sulfides from the Ronda Peridotite (Southern Spain). *Contributions to Mineralogy and Petrology*, 159(3):315—330. <https://doi.org/10.1007/s00410-009-0429-y>
- Matsumoto, T., Chen, Y.L., Matsuda, J.I., 2001. Concomitant Occurrence of Primordial and Recycled Noble Gases in the Earth's Mantle. *Earth and Planetary Science Letters*, 185(1—2):35—47. [https://doi.org/10.1016/s0012-821x\(00\)00375-7](https://doi.org/10.1016/s0012-821x(00)00375-7)
- McCuig, C.T., Kerrich, R., 1998. P-T-t-Deformation-Fluid Characteristics of Lode Gold Deposits: Evidence from Alteration Systematics. *Ore Geology Reviews*, 12(6):381—453. [https://doi.org/10.1016/s0169-1368\(98\)80002-4](https://doi.org/10.1016/s0169-1368(98)80002-4)
- Mo, X.X., Pan, G.T., 2006. From the Tethys to the Formation of the Qinghai-Tibet Plateau: Constrained by Tectono-Magmatic Events. *Earth Science Frontiers*, 13(6):43—51 (in Chinese with English abstract).
- Naden, J., Kilias, S.P., Leng, M.J., et al., 2003. Do Fluid Inclusions Preserve δ¹⁸O Values of Hydrothermal Fluids in Epithermal Systems over Geological Time? Evidence from Paleo- and Modern Geothermal Systems, Milos Island, Aegean Sea. *Chemical Geology*, 197(1—4): 143—159. [https://doi.org/10.1016/s0009-2541\(02\)00289-9](https://doi.org/10.1016/s0009-2541(02)00289-9)
- Nie, F.J., Hu, P., Jiang, S.H., et al., 2005. Type and Temporal-Spatial Distribution of Gold and Antimony Deposits (Prospects) in Southern Tibet, China. *Acta Geologica Sinica*, 79(3): 373—385(in Chinese with English abstract).
- Ohmoto, H., 1972. Systematics of Sulfur and Carbon Isotopes in Hydrothermal Ore Deposits. *Economic Geology*, 67(5): 551—578. <https://doi.org/10.2113/gsecongeo.67.5.551>
- Ohmoto, H., Rye, R.D., 1979. Isotopes of Sulfur and Carbon. In: Barnes, H.L., ed., *Geochemistry of Hydrothermal Ore Deposits*. Wiley, New York.
- Ozima, M., Podosek, F.A., 1983. *Noble Gas Geochemistry*. Cambridge University Press, Cambridge.
- Pan, G.T., Xiao, Q.H., Lu, S.N., et al., 2009. Subdivision of Tectonic Units in China. *Geology in China*, 36(1):1—28 (in Chinese with English abstract).
- Patterson, D.B., Honda, M., McDougall, I., 1994. Noble Gases in Mafic Phenocrysts and Xenoliths from New Zealand. *Geochimica et Cosmochimica Acta*, 58(20): 4411—4427. [https://doi.org/10.1016/0016-7037\(94\)90344-1](https://doi.org/10.1016/0016-7037(94)90344-1)
- Pei, Y.R., Yang, Z.S., Zhao, X.Y., et al., 2016. Sulfur and Lead Isotope Compositions of the Shangxu Orogenic Gold Deposit in Northern Tibet: Implication for the Source of Ore-Forming Material. *Acta Geologica Sinica*, 90(2):341—351(in Chinese with English abstract).
- Peters, S.G., Golding, S.D., 1989. Geologic, Fluid Inclusion, and Stable Isotope Studies of Granitoid-Hosted Gold-Bearing Quartz Veins, Charters Towers, Northeastern Australia. In: Keays, R.R., Ramsay, W.R.H., Groves, D.I., eds., *The Geology of Gold Deposits: The Perspective in 1988*. Society of Economic Geologists, 260—273. [https://doi.org/10.1016/0016-7037\(94\)90344-1](https://doi.org/10.1016/0016-7037(94)90344-1)

- //doi.org/10.5382/mono.06.20
- Petrella, L., Thébaud, N., Laflamme, C., et al., 2020. In-Situ Sulfur Isotopes Analysis as an Exploration Tool for Orogenic Gold Mineralization in the Granites-Tanami Gold Province, Australia: Learnings from the Callie Deposit. *Journal of Geochemical Exploration*, 214:106542. <https://doi.org/10.1016/j.gexplo.2020.106542>
- Pettke, T., Frei, R., 1996. Isotope Systematics in Vein Gold from Brusson, Val d' Ayas (NW Italy), 1. Pb/Pb Evidence for a Piemonte Metaophiolite Au Source. *Chemical Geology*, 127(1-3): 111–124. [https://doi.org/10.1016/0009-2541\(95\)00107-7](https://doi.org/10.1016/0009-2541(95)00107-7)
- Porcelli, D.R., O' Nions, R.K., Galer, S.J.G., et al., 1992. Isotopic Relationships of Volatile and Lithophile Trace Elements in Continental Ultramafic Xenoliths. *Contributions to Mineralogy and Petrology*, 110(4):528–538. <https://doi.org/10.1007/bf00344086>
- Qi, X.X., Li, T.F., Meng, X.J., et al., 2008. Cenozoic Tectonic Evolution of the Tethyan Himalayan Foreland Fault-Fold Belt in Southern Tibet, and Its Constraint on Antimony-Gold Polymetallic Minerogenesis. *Acta Petrologica Sinica*, 24(7):1638–1648(in Chinese with English abstract).
- Reid, M.R., Graham, D.W., 1996. Resolving Lithospheric and Sub-Lithospheric Contributions to Helium Isotope Variations in Basalts from the Southwestern US. *Earth and Planetary Science Letters*, 144(1-2):213–222. [https://doi.org/10.1016/0012-821x\(96\)00166-5](https://doi.org/10.1016/0012-821x(96)00166-5)
- Seal, R.R., 2006. Sulfur Isotope Geochemistry of Sulfide Minerals. *Reviews in Mineralogy and Geochemistry*, 61(1): 633–677. <https://doi.org/10.2138/rmg.2006.61.12>
- Shang, Q.Q., Ren, Y.S., Chen, C., et al., 2017. Metallogenic Age and Ore-Forming Material Source of Yangjin' gou Gold Deposit in Eastern Yanbian Region. *Gold*, 38(6):7–12(in Chinese with English abstract).
- Simmons, S.F., Sawkins, F.J., Schlutter, D.J., 1987. Mantle-Derived Helium in Two Peruvian Hydrothermal Ore Deposits. *Nature*, 329:429–432. <https://doi.org/10.1038/329429a0>
- Simon, K., 2001. Does δ D from Fluid Inclusion in Quartz Reflect the Original Hydrothermal Fluid? *Chemical Geology*, 177(3-4):483–495. [https://doi.org/10.1016/s0009-2541\(00\)00417-4](https://doi.org/10.1016/s0009-2541(00)00417-4)
- Stuart, F.M., Turner, G., 1992. The Abundance and Isotopic Composition of the Noble Gases in Ancient Fluids. *Chemical Geology: Isotope Geoscience Section*, 101(1-2): 97–109. [https://doi.org/10.1016/0009-2541\(92\)90207-l](https://doi.org/10.1016/0009-2541(92)90207-l)
- Stuart, F.M., Turner, G., Duckworth, R.C., et al., 1994a. Helium Isotopes as Tracers of Trapped Hydrothermal Fluids in Ocean-Floor Sulfides. *Geology*, 22(9):823–826.
- Stuart, F.M., Turner, G., Taylor, R., 1994b. He-Ar Isotope Systematics of Fluid Inclusions: Resolving Mantle and Crustal Contributions to Hydrothermal Fluids. In: Noble Gas Geochemistry and Cosmochemistry. Terra Scientific Publishing Company, 261–277.
- Sun, Q., Ren, Y.S., Li, D.X., et al., 2016. Isotopic Geochemistry and Metallogenic Material Source of Shabaosi Gold Deposit in Heilongjiang Province. *Gold*, 37(5): 10–15(in Chinese with English abstract).
- Sun, X.M., Mo, R.W., Zhai, W., et al., 2014. Infrared Fluid Inclusion Microthermometry on Stibnite from Shalagang Antimony Ore in Southern Tibet, China. *Acta Petrologica Sinica*, 30(1): 189–198(in Chinese with English abstract).
- Sun, X.M., Wei, H.X., Zhai, W., et al., 2016b. Fluid Inclusion Geochemistry and Ar-Ar Geochronology of the Cenozoic Bangbu Orogenic Gold Deposit, Southern Tibet, China. *Ore Geology Reviews*, 74: 196–210. <https://doi.org/10.1016/j.oregeorev.2015.11.021>
- Sun, X.M., Xiong, D.X., Wang, S.W., et al., 2006. Noble Gases Isotopic Composition of Fluid Inclusions in Scheelites Collected from Daping Gold Mine, Yunnan Province, China, and Its Application for Ore Genesis. *Acta Petrologica Sinica*, 22(3): 725–732(in Chinese with English abstract).
- Sun, X., Zheng, Y.Y., Wang, C.M., et al., 2016a. Identifying Geochemical Anomalies Associated with Sb-Au-Pb-Zn-Ag Mineralization in North Himalaya, Southern Tibet. *Ore Geology Reviews*, 73: 1–12. <https://doi.org/10.1016/j.oregeorev.2015.10.020>
- Tomkins, A.G., Grundy, C., 2009. Upper Temperature Limits of Orogenic Gold Deposit Formation: Constraints from the Granulite-Hosted Griffin's Find Deposit, Yilgarn Craton. *Economic Geology*, 104(5): 669–685. <https://doi.org/10.2113/gsecongeo.104.5.669>
- Torgersen, T., 1989. Terrestrial Helium Degassing Fluxes and the Atmospheric Helium Budget: Implications with Respect to the Degassing Processes of Continental Crust. *Chemical Geology: Isotope Geoscience Section*, 79:1–14. [https://doi.org/10.1016/0168-9622\(89\)90002-x](https://doi.org/10.1016/0168-9622(89)90002-x)
- Trieloff, M., Kunz, J., Allègre, C.J., 2002. Noble Gas Systematics of the Réunion Mantle Plume Source and the Origin of Primordial Noble Gases in Earth's Mantle. *Earth and Planetary Science Letters*, 200(3-4): 297–313. [https://doi.org/10.1016/s0012-821x\(02\)00639-8](https://doi.org/10.1016/s0012-821x(02)00639-8)

- Tu, G. C., 1986. Several New Advances in Earth Science in the 1980s: A Report on the 30th Anniversary of the Institute of Mineral Geology of China Non-Ferrous Metals Industry Corporation. *Geology and Prospecting*, 22(5): 1—6(in Chinese).
- Turner, G., Stuart, F., 1992. Helium/Heat Ratios and Deposition Temperatures of Sulphides from the Ocean Floor. *Nature*, 357: 581—583. <https://doi.org/10.1038/357581a0>
- Wang, Q.F., Deng, J., Weng, W.J., et al., 2020. Cenozoic Orogenic Gold System in Tibet. *Acta Petrologica Sinica*, 36(5):1315—1354(in Chinese with English abstract).
- Wang, Q.F., Deng, J., Zhao, H.S., et al., 2019. Review on Orogenic Gold Deposits. *Earth Science*, 44(6):2155—2186(in Chinese with English abstract).
- Wang, T. H., Xie, G. Q., Ye, A. W., et al., 2009. Material Sources of Gold Deposits in Xiaoqinling-Xiong'ershan Area of Western Henan Province as Well as the Relationship between Gold Deposits and Intermediate-Basic Dykes. *Acta Geoscientifica Sinica*, 30(1): 27—38(in Chinese with English abstract).
- Wei, H.X., Sun, X.M., Zhai, W., et al., 2010. He-Ar-S Isotopic Compositions of Ore-Forming Fluids in the Bangbu Large-Scale Gold Deposit in Southern Tibet, China. *Acta Petrologica Sinica*, 26(6): 1685—1691(in Chinese with English abstract).
- Wen, C.Q., Duo, J., Fan, X.P., et al., 2006. Characteristics of Ore Fluids of the Mayum Gold Deposit, Western Tibet, China. *Geological Bulletin of China*, 25(1): 261—266(in Chinese with English abstract).
- Wen, C.Q., Duo, J., Sun, Y., et al., 2004. ^{40}Ar - ^{39}Ar Dating of Quartz from Gold-Bearing Quartz Veins in the Mayum Gold Deposit, Burang, Tibet, and Its Geological Significance. *Regional Geology of China*, 23(7): 686—688(in Chinese with English abstract).
- Wu, F.Y., Liu, X.C., Liu, Z.C., et al., 2020. Highly Fractionated Himalayan Leucogranites and Associated Rare-Metal Mineralization. *Lithos*, 352—353: 105319. <https://doi.org/10.1016/j.lithos.2019.105319>
- Wu, F.Y., Liu, Z.C., Liu, X.C., et al., 2015. Himalayan Leucogranite: Petrogenesis and Implications to Orogenesis and Plateau Uplift. *Acta Petrologica Sinica*, 31(1): 1—36(in Chinese with English abstract).
- Wu, J. Y., Li, G. M., Zhou, Q., et al., 2015. A Preliminary Study of the Metallogenetic System in the Zhaxikang Integrated Exploration Area, Southern Tibet. *Geology in China*, 42(6): 1674—1683(in Chinese with English abstract).
- Xiang, A.P., Li, W.C., Li, G.M., et al., 2020. Mineralogy, Isotope Geochemistry and Ore Genesis of the Miocene Cuonadong Leucogranite-Related Be-W-Sn Skarn Deposit in Southern Tibet. *Journal of Asian Earth Sciences*, 196: 104358. <https://doi.org/10.1016/j.jseas.2020.104358>
- Xie, L., Tao, X.Y., Wang, R.C., et al., 2020. Highly Fractionated Leucogranites in the Eastern Himalayan Cuonadong Dome and Related Magmatic Be-Nb-Ta and Hydrothermal Be-W-Sn Mineralization. *Lithos*, 354—355: 105286. <https://doi.org/10.1016/j.lithos.2019.105286>
- Xie, Y.L., Li, L.M., Wang, B.G., et al., 2017. Genesis of the Zhaxikang Epithermal Pb-Zn-Sb Deposit in Southern Tibet, China: Evidence for a Magmatic Link. *Ore Geology Reviews*, 80: 891—909. <https://doi.org/10.1016/j.oregeorev.2016.08.007>
- Xie, Y.L., Yang, K.J., Li, Y.X., et al., 2019. Mazhala Gold-Antimony Deposit in Southern Tibet: The Characteristics of Ore-Forming Fluids and the Origin of Gold and Antimony. *Earth Science*, 44(6): 1998—2016(in Chinese with English abstract).
- Yang, Z. S., Hou, Z. Q., Gao, W., et al., 2006. Metallogenetic Characteristics and Genetic Model of Antimony and Gold Deposits in South Tibetan Detachment System. *Acta Geologica Sinica*, 80(9): 1377—1391(in Chinese with English abstract).
- Yang, Z.S., Hou, Z.Q., Meng, X.J., et al., 2009. Post-Colli- sional Sb and Au Mineralization Related to the South Tibetan Detachment System, Himalayan Orogen. *Ore Geology Reviews*, 36(1—3): 194—212. <https://doi.org/10.1016/j.oregeorev.2009.03.005>
- Yuan, H.L., Liu, X., Chen, L., et al., 2018. Simultaneous Measurement of Sulfur and Lead Isotopes in Sulfides Using Nanosecond Laser Ablation Coupled with Two Multi-Collector Inductively Coupled Plasma Mass Spectrometers. *Journal of Asian Earth Sciences*, 154: 386—396. <https://doi.org/10.1016/j.jseas.2017.12.040>
- Zhai, W., Sun, X. M., Wu, Y. S., et al., 2012. He-Ar Isotope Geochemistry of the Yaoling-Meizivo Tungsten Deposit, North Guangdong Province: Constraints on Yanshabian Crust-Mantle Interaction and Metallogenesis in SE China. *Chinese Science Bulletin*, 57(13): 1137—1146(in Chinese).
- Zhai, W., Zheng, S.Q., Sun, X.M., et al., 2018. He-Ar Isotope Compositions of Orogenic Mazhala Au-Sb and Shalagang Sb Deposits in Himalayan Orogeny, Southern Tibet: Constraints to Ore-Forming Fluid Origin. *Acta Petrologica Sinica*, 34(12): 3525—3538(in Chinese with English abstract).

- Zhang, G. Y., 2012. Metallogenetic Model and Prospecting Potential in Southern Tibet Au-Sb Polymetallic Belt (Dissertation). China University of Geosciences, Wuhan (in Chinese with English abstract).
- Zhang, J.F., Zheng, Y.Y., Zhang, G.Y., et al., 2011. Geologic Characteristic and Mineralization of Mazhala Gold-Antimony Deposit in Northern Himalaya. *Gold*, 32(1): 20–24(in Chinese with English abstract).
- Zhang, J.J., 2007. A Review on the Extensional Structures in the Northern Himalaya and Southern Tibet. *Geological Bulletin of China*, 26(6):639–649(in Chinese with English abstract).
- Zhang, J.J., Ding, L., 2003. East-West Extension in Tibetan Plateau and Its Significance to Tectonic Evolution. *Scientia Geologica Sinica*, 38(2): 179–189(in Chinese with English abstract).
- Zhang, J.J., Guo, L., Zhang, B., 2007. Structure and Kinematics of the Yalashangbo Dome in the Northern Himalayan Dome Belt, China. *Chinese Journal of Geology (Scientia Geologica Sinica)*, 42(1):16–30(in Chinese with English abstract).
- Zhang, L.K., Li, G.M., Cao, H.W., et al., 2019. Zircon Geochronology and Hf Isotope Compositions of the Granitic Gneiss from Cuonadong in South Tibet and Its Insights for the Evolution of the Proto-Tethys. *Geology in China*, 46(6):1312–1335(in Chinese with English abstract).
- Zhang, L.K., Zhang, Z., Li, G.M., et al., 2018. Rock Assemblage, Structural Characteristics and Genesis Mechanism of the Cuonadong Dome, Tethys Himalaya. *Earth Science*, 43(8): 2664–2683(in Chinese with English abstract).
- Zhang, X., 2017. Mineralization of Orogenic Gold Deposits in the Indus-Yarlung' Tsangpo Suture Zone of Tibetan Plateau (Dissertation). China University of Geosciences, Beijing(in Chinese with English abstract).
- Zhang, Z., Li, G.M., Zhang, L.K., et al., 2020. Genesis of the Mingsai Au Deposit, Southern Tibet: Constraints from Geology, Fluid Inclusions, $^{40}\text{Ar}/^{39}\text{Ar}$ Geochronology, H-O Isotopes, and In Situ Sulfur Isotope Compositions of Pyrite. *Ore Geology Reviews*, 122: 103488. <https://doi.org/10.1016/j.oregeorev.2020.103488>
- Zhao, J., Liang, J.L., Li, J., et al., 2018. Genesis and Metallogenetic Model of the Shuiyindong Gold Deposit, Guizhou Province: Evidences from High-Resolution Multi-Element Mapping and In Situ Sulfur Isotopes of Au-Carrying Pyrites by NanoSIMS. *Earth Science Frontiers*, 25(1):157–167(in Chinese with English abstract).
- Zhao, Z.F., Chen, R.X., Chen, Y.X., et al., 2021. Progresses in the Study of Partial Melting of Ultrahigh-Pressure Metamorphic Rocks and Crust-Mantle Interaction in Continental Subduction Zones. *Bulletin of Mineralogy, Petrology and Geochemistry*, 40(1): 36–59(in Chinese with English abstract).
- Zheng, S.H., Zhang, Z.F., Ni, B.L., et al., 1982. Hydrogen and Oxygen Isotopic Studies of Thermal Waters in Xizang. *Acta Scientiarum Naturalium Universitatis Pekinesis*, 18(1):99–106(in Chinese with English abstract).
- Zheng, Y.Y., Zhao, Y.X., Wang, P., et al., 2004. Great Progress has been Made on Metallogenetic Regularities and Ore-Prospecting in the Gold-Antimony Metallogenetic Belt, South Tibet. *Earth Science*, 29(1):44, 68(in Chinese with English abstract).
- Zhou, F., Sun, X.M., Zhai, W., et al., 2014. Helium and Argon Isotope Geochemistry of Ore-Forming Fluids in Zhemulang Gold Deposit in Southern Tibet, China. *Acta Geologica Sinica*, 88(Suppl. 2): 860–861. https://doi.org/10.1111/1755-6724.12375_88
- Zhou, Y., Wang, X. W., Tang, J. X., et al., 2011. Origin and Evolution of Ore-Forming Fluids from Jiama Copper Polymetallic Deposit in Tibet. *Mineral Deposits*, 30(2): 231–248(in Chinese with English abstract).
- Zhu, D.C., Chung, S.L., Mo, X.X., et al., 2009. The 132 Ma Comei-Bunbury Large Igneous Province: Remnants Identified in Present-Day Southeastern Tibet and Southwestern Australia. *Geology*, 37(7):583–586. <https://doi.org/10.1130/g30001a.1>
- Zhu, D.C., Zhao, Z.D., Niu, Y.L., et al., 2011. Lhasa Terrane in Southern Tibet Came from Australia. *Geology*, 39(8): 727–730. <https://doi.org/10.1130/g31895.1>
- Zhu, F. S., 1982. Discussion on the Genetic Classification of Gold Deposits. *Gold*, 3(1):21–26(in Chinese).
- Zhu, Z.X., Zhao, X.F., Lin, Z.W., et al., 2020. In Situ Trace Elements and Sulfur Isotope Analysis of Pyrite from Jinchiling Gold Deposit in the Jiaodong Region: Implications for Ore Genesis. *Earth Science*, 45(3): 945–959(in Chinese with English abstract).

附中文参考文献

- 陈翠华,赵德坤,顾雪祥,等,2014.云南老寨湾金矿床成矿物质来源探讨.矿物岩石地球化学通报,33(1):23–30.
- 陈衍景,富士谷,卢冰,等,1992.金矿成因类型和系列的划分.地球科学进展,7(3):73–79.
- 陈衍景,倪培,范宏瑞,等,2007.不同类型热液金矿系统的流体包裹体特征.岩石学报,23(9):2085–2108.
- 丁辉,葛文胜,董连慧,等,2018.新疆东准噶尔绿源金矿床地质特征与金成矿物质来源分析.地质学报,92(5):

- 1019—1040.
- 董随亮,黄勇,李光明,等,2017.藏南姐纳各普金矿地质特征及成矿时代约束:对扎西康矿集区铅锌金锑成矿系统的启示.资源与产业,19(5):56—64.
- 付建刚,李光明,王根厚,等,2018.北喜马拉雅双穹隆构造的建立:来自藏南错那洞穹隆的厘定.中国地质,45(4):783—802.
- 郭春影,张文钊,葛良胜,等,2011.氢氧同位素体系成矿流体示踪若干问题.矿物岩石,31(3):41—47.
- 侯增谦,莫宣学,杨志明,等,2006b.青藏高原碰撞造山带成矿作用:构造背景、时空分布和主要类型.中国地质,33(2):340—351.
- 侯增谦,曲晓明,杨竹森,等,2006a.青藏高原碰撞造山带:Ⅲ.后碰撞伸展成矿作用.矿床地质,25(6):629—651.
- 侯增谦,王二七,2008.印度—亚洲大陆碰撞成矿作用主要研究进展.地球学报,29(3):275—292.
- 侯增谦,杨竹森,徐文艺,等,2006c.青藏高原碰撞造山带:I.主碰撞造山成矿作用.矿床地质,25(4):337—358.
- 胡瑞忠,1997.成矿流体氦、氩同位素地球化学.矿物岩石地球化学通报,16(2):52—56.
- 黄春梅,李光明,张志,等,2018.藏南错那洞淡色花岗岩成因:来自全岩地球化学和锆石U-Pb年龄的约束.地学前缘,25(6):182—195.
- 李光明,张林奎,焦彦杰,等,2017.西藏喜马拉雅成矿带错那洞超大型铍锡钨多金属矿床的发现及意义.矿床地质,36(4):1003—1008.
- 李洪梁,2016.西藏扎西康矿集区姐纳各普金矿构造背景与矿床成因研究(硕士学位论文).成都:成都理工大学.
- 李洪梁,2020.特提斯喜马拉雅东段扎西康矿集区造山型金矿床成矿作用研究(博士学位论文).成都:成都理工大学.
- 李洪梁,李光明,2019.不同类型热液金矿床主成矿期黄铁矿成分标型特征.地学前缘,26(3):202—210.
- 李洪梁,李光明,丁俊,等,2020.藏南扎西康铅锌多金属矿床成因:硫化物原位硫同位素证据.吉林大学学报(地球科学版),50(5):1289—1303.
- 李洪梁,李光明,李应彬,等,2017.藏南扎西康矿集区姐纳各普金矿床地质与流体包裹体特征.矿物学报,37(6):684—696.
- 李洪梁,李光明,张志,等,2016.藏南扎西康铅锌多金属矿床控矿因素及找矿预测.金属矿山,(10):103—108.
- 李杰,申俊峰,李金春,等,2016.甘肃岗岔金矿床同位素地球化学特征及成矿物质来源探讨.矿物岩石地球化学通报,35(5):976—983.
- 梁维,2014.特提斯喜马拉雅金锑铅锌成矿带成矿作用研究(博士学位论文).北京:中国地质大学(北京).
- 梁维,郑远川,2019.藏南吉松铅锌矿成矿时代的厘定:热液绢云母Ar-Ar年龄.中国地质,46(1):126—139.
- 刘伟,李新俊,邓军,2002.东天山金窝子石英脉金矿床成矿流体和成矿物质的来源.中国科学:地球科学,32(增刊1):105—119.
- 卢焕章,2008.CO₂流体与金矿化:流体包裹体的证据.地球化学,37(4):321—328.
- 卢焕章,池国祥,朱笑青,等,2018.造山型金矿的地质特征和成矿流体.大地构造与成矿学,42(2):244—265.
- 卢柳,2019.西藏隆子县明赛金矿矿床地质特征及其成因初探(硕士学位论文).成都:成都理工大学.
- 毛景文,李晓峰,2004.深部流体及其与成矿成藏关系研究现状.矿床地质,23(4):520—532.
- 莫宣学,潘桂棠,2006.从特提斯到青藏高原形成:构造—岩浆事件的约束.地学前缘,13(6):43—51.
- 聂凤军,胡朋,江思宏,等,2005.藏南地区金和锑矿床(点)类型及其时空分布特征.地质学报,79(3):373—385.
- 潘桂棠,肖庆辉,陆松年,等,2009.中国大地构造单元划分.中国地质,36(1):1—28.
- 裴英茹,杨竹森,赵晓燕,等,2016.藏北商旭金矿床S、Pb同位素组成:对成矿物质来源的指示.地质学报,90(2):341—351.
- 戚学祥,李天福,孟祥金,等,2008.藏南特提斯喜马拉雅前陆断褶带新生代构造演化与锑金多金属成矿作用.岩石学报,24(7):1638—1648.
- 商青青,任云生,陈聪,等,2017.延边东部杨金沟金矿床成矿时代与成矿物质来源.黄金,38(6):7—12.
- 孙琦,任云生,李德新,等,2016.黑龙江省砂宝斯金矿床同位素地球化学特征与成矿物质来源.黄金,37(5):10—15.
- 孙晓明,莫儒伟,翟伟,等,2014.藏南沙拉岗锑矿流体包裹体红外显微测温研究.岩石学报,30(1):189—198.
- 孙晓明,熊德信,王生伟,等,2006.云南大坪金矿白钨矿惰性气体同位素组成及其成矿意义.岩石学报,22(3):725—732.
- 涂光炽,1986.八十年代地球科学的若干新进展:在中国有色金属工业总公司矿产地质研究院三十周年院庆活动中的报告.地质与勘探,22(5):1—6.
- 王庆飞,邓军,翁伟俊,等,2020.青藏高原新生代造山型金成矿系统.岩石学报,36(5):1315—1353.
- 王庆飞,邓军,赵鹤森,等,2019.造山型金矿研究进展:兼论中国造山型金成矿作用.地球科学,44(6):2155—2186.
- 王团华,谢桂青,叶安旺,等,2009.豫西小秦岭—熊耳山地区金矿成矿物质来源研究:兼论中基性岩墙与金成矿作用关系.地球学报,30(1):27—38.
- 韦慧晓,孙晓明,翟伟,等,2010.藏南邦布大型金矿成矿流体He-Ar-S同位素组成及其成矿意义.岩石学报,26(6):1685—1691.
- 温春齐,多吉,范小平,等,2006.西藏西部马攸木金矿床成矿流体的特征.地质通报,25(1):261—266.
- 温春齐,多吉,孙燕,等,2004.西藏普兰县马攸木金矿床石英

- 的⁴⁰Ar/³⁹Ar年龄及其地质意义.地质通报,23(7):686—688.
- 吴福元,刘志超,刘小驰,等,2015.喜马拉雅淡色花岗岩.岩石学报,31(1):1—36.
- 吴建阳,李光明,周清,等,2015.藏南扎西康整装勘查区成矿体系初探.中国地质,42(6):1674—1683.
- 谢玉玲,杨科君,李应栩,等,2019.藏南马扎拉金—锑矿床:成矿流体性质和成矿物质来源.地球科学,44(6):1998—2016.
- 杨竹森,侯增谦,高伟,等,2006.藏南拆离系锑金成矿特征与成因模式.地质学报,80(9):1377—1391.
- 张刚阳,2012.藏南金锑多金属成矿带成矿模式与找矿前景研究(博士学位论文).武汉:中国地质大学.
- 张建芳,郑有业,张刚阳,等,2011.西藏北喜马拉雅马扎拉金锑矿床地质特征及成矿作用.黄金,32(1):20—24.
- 张进江,2007.北喜马拉雅及藏南伸展构造综述.地质通报,26(6):639—649.
- 张进江,丁林,2003.青藏高原东西向伸展及其地质意义.地质科学,38(2):179—189.
- 张进江,郭磊,张波,2007.北喜马拉雅穹隆带雅拉香波穹隆的构造组成和运动学特征.地质科学,42(1):16—30.
- 张林奎,李光明,曹华文,等,2019.藏南错那洞花岗质片麻岩锆石年龄、Hf同位素及其对原特提斯洋演化的启示.中国地质,46(6):1312—1335.
- 张林奎,张志,李光明,等,2018.特提斯喜马拉雅错那洞穹隆的岩石组合、构造特征与成因.地球科学,43(8):2664—2683.
- 张雄,2017.青藏高原雅鲁藏布江缝合带造山型金矿成矿作用研究(博士学位论文).北京:中国地质大学.
- 翟伟,孙晓明,邬云山,等,2012.粤北瑶岭—梅子窝钨矿He-Ar同位素地球化学:对华南燕山期壳幔作用过程与成矿的制约.科学通报,57(13):1137—1146.
- 翟伟,郑思琦,孙晓明,等,2018.藏南喜马拉雅造山带造山型马扎拉Au-Sb矿床和沙拉岗Sb矿床流体包裹体He-Ar同位素组成:对成矿流体来源的制约.岩石学报,34(12):3525—3538.
- 赵静,梁金龙,李军,等,2018.贵州贞丰水银洞金矿矿床成因与成矿模式:来自载金黄铁矿NanoSIMS多元素Mapping及原位微区硫同位素的证据.地学前缘,25(1):157—167.
- 赵子福,陈仁旭,陈伊翔,等,2021.大陆俯冲带超高压变质岩部分熔融与壳幔相互作用研究进展.矿物岩石地球化学通报,40(1):36—59.
- 郑淑蕙,张知非,倪葆龄,等,1982.西藏地热水的氢氧稳定同位素研究.北京大学学报(自然科学版),18(1):99—106.
- 郑有业,赵永鑫,王萍,等,2004.藏南金锑成矿带成矿规律研究及找矿取得重大进展.地球科学,29(1):44,68.
- 周云,汪雄武,唐菊兴,等,2011.西藏甲玛铜多金属矿床成矿流体来源及演化.矿床地质,30(2):231—248.
- 朱奉三,1982.金矿床成因类型划分的讨论.黄金,3(1):21—26,65.
- 朱照先,赵新福,林祖苇,等,2020.胶东金翅岭金矿床黄铁矿原位微量元素和硫同位素特征及对矿床成因的指示.地球科学,45(3):945—959.